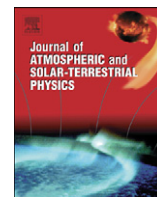




Contents lists available at SciVerse ScienceDirect

Journal of Atmospheric and Solar-Terrestrial Physics

journal homepage: www.elsevier.com/locate/jastp

Cosmogenic ^7Be and ^{22}Na in Finland: Production, observed periodicities and the connection to climatic phenomena

A.-P. Leppänen^{a,*}, I.G. Usoskin^b, G.A. Kovaltsov^c, J. Paatero^d

^a Radiation and Nuclear Safety Authority, Regional Laboratory in Northern Finland, Rovaniemi, Finland

^b Sodankylä Geophysical Observatory, Oulu Unit, University of Oulu, Finland

^c Ioffe Physical-Technical Institute, St. Petersburg, Russia

^d Finnish Meteorological Institute, Observation Services, Helsinki, Finland

ARTICLE INFO

Article history:

Received 14 February 2011

Received in revised form

11 August 2011

Accepted 21 October 2011

Available online 15 November 2011

Keywords:

^7Be

^{22}Na

Cosmic rays

Atmosphere

Teleconnections

Finland

ABSTRACT

This study presents theoretical production calculations and time series analyses of two cosmogenic isotopes, ^7Be and ^{22}Na , from the four high-latitude stations of Kotka, Kajaani, Rovaniemi and Ivalo located in Finland. We used published results for ^7Be but performed full simulations of the ^{22}Na production in atmosphere. For the first time, lookup tables of ^{22}Na production by cosmic rays in the atmosphere are presented. In conjunction with calculations using the new model of ^{22}Na production, the $^7\text{Be}/^{22}\text{Na}$ ratios in the atmosphere were also calculated. The wavelet transform of the ^7Be and ^{22}Na time series revealed sets of periodicities in the 2.5–8 year range. The wavelet coherence method was used to study coherences between ^7Be and ^{22}Na and $^7\text{Be}/^{22}\text{Na}$ data and AO, NAO, AMO, QBO and SO teleconnection indices representing different climatic variations in Northern Europe. In the wavelet coherence analyses, the ^7Be activities were found to be mainly modulated by NAO and AMO at an interannual scale, while ^{22}Na activity was found to be less effected by climatic phenomena. The ^7Be coherence with other indices was intermittent where the coherence with SO was limited to Ivalo data and in the case of QBO, to Kotka data. The ^{22}Na data was not found to be in coherence with any of the studied indices. In the $^7\text{Be}/^{22}\text{Na}$ ratio a clear seasonal pattern was observed where low $^7\text{Be}/^{22}\text{Na}$ ratios were observed during summer and high ratios during winter. This was speculated to be caused by the height of atmospheric vertical mixing. During 2006–2011, the $^7\text{Be}/^{22}\text{Na}$ ratios from Kotka, Kajaani and Rovaniemi showed variance at synoptic time scales but were nearly identical at the seasonal scale. The $^7\text{Be}/^{22}\text{Na}$ ratio was proposed to be a radiochronometer to estimate residence times of aerosols carrying ^7Be and ^{22}Na .

© 2011 Elsevier Ltd. All rights reserved.

1. Introduction

Cosmogenic nuclides have been used in many applications from palaeoclimatology to solar activity reconstructions. In particular, the ratio of the cosmogenic isotopes produced in spallation reactions, such as ^7Be and ^{22}Na , has been found to be a useful tool for studying atmospheric processes (e.g., Bhandari et al., 1966; Tokuyama and Igarashi, 1998; Jasiulionis and Wershofen, 2005). One of the most studied cosmogenic isotopes is ^7Be , while ^{22}Na is significantly less known. The ^7Be isotope is formed in the galactic cosmic-ray-induced spallation of atmospheric nitrogen and oxygen while ^{22}Na is produced in the spallation of atmospheric argon. These cosmogenic isotopes are radioactive having different half-lives, ^7Be $T_{1/2}=53.22$ d and ^{22}Na $T_{1/2}=2.603$ years. ^7Be is

abundant in ambient air where typical activity concentration varies from few hundred to few thousand $\mu\text{Bq}/\text{m}^3$. Compared to ^7Be , the activity concentrations of ^{22}Na are roughly four orders of magnitude lower, typically below $1 \mu\text{Bq}/\text{m}^3$ (Grabowska et al., 2003; Jasiulionis and Wershofen, 2005; Rulík et al., 2009). This is mainly due to low concentrations and higher spallation threshold energy of atmospheric argon ($E_T \approx 200$ MeV) compared to oxygen ($E_T \approx 30$ MeV).

The concentrations of cosmogenic nuclides in ground level air are, despite production changes, dependent on four factors: (1) wet scavenging, (2) stratosphere-to-troposphere exchange, (3) vertical transfer in troposphere and (4) horizontal transfer between different latitudes (Feely et al., 1989). About 75% of ^7Be is produced in the stratosphere and 25% in the upper troposphere (Johnson and Viezee, 1981; Usoskin and Kovaltsov, 2008). The chemical properties of ^7Be and ^{22}Na differ from each other. However, these differences should not affect their behavior in the upper troposphere or stratosphere. After formation and adsorption onto local

* Corresponding author. Tel.: +358 40 7641788.

E-mail address: ari.leppanen@stuk.fi (A.-P. Leppänen).

aerosols ^7Be and ^{22}Na are transported to ground level via atmospheric vertical mixing (Lal and Peters, 1962; Vecchi and Valli, 1997). ^7Be attaches predominantly to aerosols of the (sub)micron size (El-Hussein and Ahmed, 1994; Papastefanou and Ioannidou, 1995). Thus their behavior, excluding radioactive decay, is governed by the dynamics, transport and removal processes of the aerosol particles carrying them. ^7Be was already proposed as a natural atmospheric tracer in the late 1950s (Lal et al., 1958). However, the use of ^7Be as an atmospheric tracer is difficult due to the complexity of atmospheric processes affecting ground-level concentrations. Recently, a cosmic ray model was combined with an atmospheric model enabling novel possibilities to study ^7Be as an atmospheric tracer in more detail (Usoskin and Kovaltsov, 2008; Usoskin et al., 2009).

The ambient air ^7Be and ^{22}Na activity can be largely affected by seasonal variability. The effect of particularly spring and/or autumn stratospheric-tropospheric mixing on ambient air ^7Be activity concentrations has been studied widely, see e.g. Feely et al. (1989), Gerasopoulos et al. (2003), and Aldahan et al. (2008). In addition, the concentrations of ^7Be are known to be modulated by large-scale atmospheric phenomena (NAO and ENSO) and by the 11-year solar cycle (see e.g. Koch and Mann, 1996; Talpos et al., 2005; Kikuchi et al., 2009; Leppänen et al., 2010). The seasonal cycle in ^{22}Na activities has been studied from aerosol samples and monthly radioactivity measurements of rainfall (Tokuyama and Igarashi, 1998; Leppänen and Grinsted, 2008; Rulík et al., 2009). Finland is located in the transition zone between continental Eurasia and the North Atlantic. Westerly winds that transport maritime air from the Atlantic region are common. These winds generally carry low concentrations of ^7Be partly due to significant wet and dry depositions in the North Atlantic along the path of the Gulf Stream (Field et al., 2006). In Northern Finland, the source areas of ^7Be -rich air are in Central Russia and, in the springtime, in the southwest of Finland (Paatero and Hatakka, 2000). Thus depending on the origin of air masses, different ^7Be and ^{22}Na activity concentrations are observed.

2. Production of ^7Be and ^{22}Na in the atmosphere

2.1. Modeling of the isotope production in the atmosphere

Several models have been published earlier (Lal and Peters, 1962; O'Brien, 1979; Masarik and Beer, 1999; Luyanas, 2004; Webber et al., 2007) to calculate the production rates for these isotopes in the atmosphere. These earlier models do not provide a 3D picture of the isotope production over the wide range of solar activity variations, which is necessary to study the details of the production and transport. Moreover, many of the earlier models are based on simplified assumptions thus reducing their accuracy, especially in the lower atmosphere. Nowadays, the production of cosmogenic isotopes can be modeled by a specially developed code, CRAC (Cosmic Ray induced Atmospheric Cascade), originally built for the beryllium isotopes ^7Be and ^{10}Be (Usoskin and Kovaltsov, 2008; Kovaltsov and Usoskin, 2010). Since ^{22}Na is produced in a similar way to beryllium isotopes, i.e., in the spallation of atmospheric argon nuclei, we can also apply the same approach, called CRAC:22Na. Here we only briefly describe some details for the sodium isotope, while full details of the model are given elsewhere (Usoskin and Kovaltsov, 2008; Kovaltsov and Usoskin, 2010).

The cosmogenic isotope ^{22}Na is produced in the atmosphere mainly as a result of the spallation of nuclei of atmospheric argon by energetic protons, neutrons and α -particles. These energetic particles can be either primary cosmic rays in the upper atmosphere or secondary nucleonic components of the cascade

initiated by interactions of cosmic rays in the atmosphere. We have modeled the development of the atmospheric cascade by means of a Monte-Carlo simulation tool CORSIKA (Cosmic Ray Simulations for Cascade, version 6.617, August 2007) (Heck et al., 1998) linked to the FLUKA tool (version 2006.3b, March 2007) (Fassò et al., 2001) to simulate interactions between low energy (below 80 GeV of total energy) hadrons, as described by Kovaltsov and Usoskin (2010). The chemical composition of the atmosphere was taken as N_2 , O_2 and Ar in the volume fractions of 78.1%, 21% and 0.9%, respectively.

The efficiency of the ^{22}Na isotope production in air by a particle (p , n or α) with the kinetic energy per nucleon E

$$S_x(E) = \kappa_{\text{Ar}} \cdot \sigma_{x\text{Ar}}(E), \quad (1)$$

where x is the type of impinging particle (proton p , neutron n or α -particle), $\sigma_{x\text{Ar}}$ is the cross section of ^{22}Na production by particle of type x on argon, $\kappa_{\text{Ar}} = 1.94 \times 10^{20} \text{ g}^{-1}$ is the numbers of argon atoms per gram of air.

A cross-section for protons $\sigma_{p\text{Ar}}$ has been adopted from Reys et al. (1981). We found no information on the cross-section for neutrons and assumed $\sigma_{n\text{Ar}} \approx \sigma_{p\text{Ar}}$, which is in accordance with the high spallation threshold. Following Silberberg and Tsao (1973) and Tatischeff et al. (2006), we consider that $\sigma_{\alpha\text{Ar}}(E) = 2\sigma_{p\text{Ar}}(4E)$. The corresponding efficiencies of ^7Be and ^{22}Na are shown in Fig. 1.

As the next step we computed the yield function, which is defined as the production of the isotope by primary particles of type X with the unit intensity J (i.e., one primary particle with

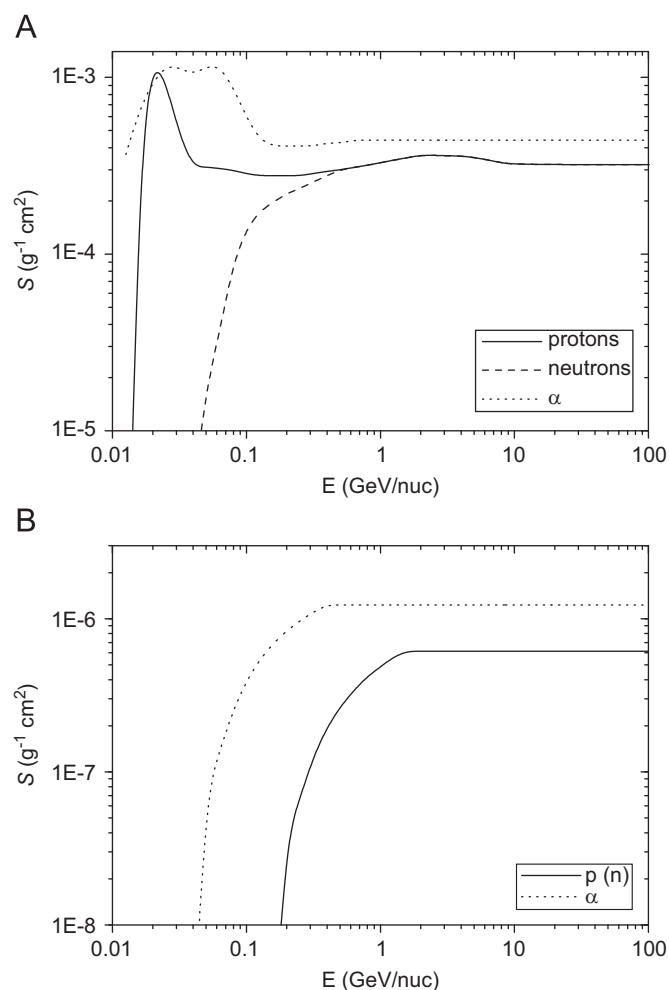


Fig. 1. Efficiency of production of cosmogenic isotopes ^7Be (panel A—cf. Fig. 1 in Usoskin and Kovaltsov, 2008) and ^{22}Na (panel B) in air.

energy E_0 in the interplanetary space per steradian per sec per cm^2). The units of Y are ($\text{atoms g}^{-1} \text{cm}^2 \text{sr}$). The tabulated yield functions of ^{22}Na production are presented in Tables 1 and 2 for primary cosmic protons and α -particles, respectively. The isotope production is given per nucleon of the incident primary particle, i.e., the production by one α -particle is four times that shown here.

Production of ^{22}Na in the atmosphere can be computed using the yield function in a similar way to other cosmogenic isotopes (Usoskin and Kovaltsov, 2008). The production of the isotope Q at a given atmospheric level h and geomagnetic cutoff rigidity P_c can be computed as a sum (over different species of cosmic rays) of integrals over the energy of primary cosmic rays E_0

$$Q(h, \phi, P_c) = \sum_x Q_x = \sum_i \int_{E_{c,x}}^{\infty} J_x(E_0, \phi) Y_x(h, E_0) dE_0, \quad (2)$$

where Y_x is the yield function and J_x is the differential energy spectrum of the x th specie of galactic cosmic rays (protons and α -particles here). The spectrum of GCRs at the Earth's orbit is parameterized by the force-field approximation with its only variable parameter modulation potential ϕ (Usoskin et al., 2005). Integration is over the kinetic energy above $E_{c,x}$, which is the kinetic energy corresponding to the local vertical geomagnetic rigidity cutoff P_c , related to the local geomagnetic coordinates (Cooke et al., 1991).

By means of the above formalism, one can easily compute the ^{22}Na production rate for a given altitude h , location P_c and time (or actually, the modulation potential ϕ), using the following scheme: (1) tabulated values of the yield function $Y(E_0, h)$ are given in Tables 1 and 2 for protons and α -particles, respectively; (2) the value of the modulation potential ϕ can be obtained for a

given period from Usoskin (2005, 2011) or from a continuously updated list at <http://cosmicrays.oulu.fi/phi>; (3) the final production rate is computed using Eq. (2).

The columnar average production rate is shown in Table 3B for three levels of the solar activity (minimum $\phi = 300$ MV, medium 650 MV and maximum 1000 MV). We computed the production rate separately for the troposphere and stratosphere (their sum implies the total atmospheric columnar production rate), considering the annual mean realistic tropopause profile, similar to Kovaltsov and Usoskin (2010). We considered two cases: polar (above 60° of geographic latitude) and global (all latitudes) production. Our global mean columnar production rate is well in agreement with the earlier estimates of $\approx 5.6 \times 10^{-5}$ atoms/ cm^2/s for the average columnar production of ^{22}Na (Lal and Peters, 1962; Luyanas, 2004). Block A of the same Table shows the corresponding columnar production of ^7Be computed using the CRAC:7Be model (Usoskin and Kovaltsov, 2008).

Block C gives the values of the $^7\text{Be}/^{22}\text{Na}$ production ratio. The ratio varies between 1200 for the total atmosphere up to 2300 for the polar troposphere at solar minimum. The values computed here are in general agreement with the ratio computed earlier using a semi-empirical approach (Lal and Peters, 1962; Jasiulionis and Wershofen, 2005). We note that, on the one hand, while the production rate of each isotope is sensitive to the level of solar activity (during solar maximum it is half of that for the solar minimum), the ratio is stable, varying by less than 10% over the solar cycle. On the other hand the ratio is very sensitive to altitude, as one can see from Fig. 2. It varies by a factor of two between the middle stratosphere and sea level. This is caused by the very different energy thresholds for production of the two isotopes (Fig. 1). In the lower layers of the atmosphere, secondary

Table 1
Yield function Y_p/π of ^{22}Na production (in atoms $\text{g}^{-1} \text{cm}^2$) by primary cosmic protons with the energy given in GeV/nuc (columns 2–14). Column 1 depicts the atmospheric depth h in g/cm^2 .

h/E_0	0.05	0.1	0.15	0.4	0.76	1.9	4.6	10.0	21.5	46.4	100
1	0	0	3.9E-09	3.9E-07	8.4E-07	1.2E-06	1.2E-06	1.2E-06	1.2E-06	1.2E-06	1.2E-06
10	0	0	0	2.3E-07	6.5E-07	1.0E-06	1.2E-06	1.4E-06	1.4E-06	1.5E-06	1.5E-06
20	0	0	0	1.6E-07	5.3E-07	9.0E-07	1.2E-06	1.3E-06	1.4E-06	1.6E-06	1.6E-06
45	0	0	0	4.1E-08	3.0E-07	7.4E-07	1.0E-06	1.3E-06	1.5E-06	1.7E-06	1.8E-06
100	0	0	0	7.0E-09	8.0E-08	4.3E-07	8.0E-07	1.1E-06	1.3E-06	1.7E-06	1.9E-06
200	0	0	0	1.2E-09	1.2E-08	1.6E-07	3.8E-07	6.0E-07	8.5E-07	1.2E-06	1.4E-06
300	0	0	0	4.0E-10	3.8E-09	6.0E-08	1.9E-07	3.3E-07	5.0E-07	7.5E-07	1.0E-06
400	0	0	0	1.4E-10	1.5E-09	2.3E-08	9.1E-08	1.6E-07	2.6E-07	4.2E-07	5.8E-07
500	0	0	0	5.2E-11	5.3E-10	8.5E-09	4.3E-08	7.5E-08	1.3E-07	2.3E-07	3.5E-07
700	0	0	0	1.7E-11	1.2E-10	1.4E-09	8.8E-09	1.7E-08	3.3E-08	6.3E-08	1.0E-07
850	0	0	0	1.0E-11	6.8E-11	4.9E-10	2.7E-09	6.2E-09	1.2E-08	2.2E-08	4.2E-08
1000	0	0	0	7.2E-12	4.0E-11	2.4E-10	1.1E-09	2.3E-09	4.0E-09	8.3E-09	1.5E-08

Table 2
Yield function Y_α/π of ^{22}Na production (in atoms $\text{g}^{-1} \text{cm}^2$) by primary cosmic α -particles (per nucleon) with the energy given in GeV/nuc (columns 2–14). Column 1 depicts the atmospheric depth h in g/cm^2 .

h/E_0	0.05	0.1	0.15	0.4	0.76	1.9	4.6	10.0	21.5	46.4	100
1	1.4E-07	7.8E-07	1.1E-06	1.4E-06	2.5E-06						
10	0	0	1.6E-07	4.0E-07	8.0E-07	1.2E-06	1.5E-06	1.7E-06	1.9E-06	2.0E-06	2.0E-06
20	0	0	0	2.3E-07	5.0E-07	9.0E-07	1.2E-06	1.5E-06	1.7E-06	1.9E-06	1.9E-06
45	0	0	0	9.1E-08	2.6E-07	5.7E-07	8.7E-07	1.2E-06	1.4E-06	1.7E-06	1.7E-06
100	0	0	0	2.0E-08	1.0E-07	3.5E-07	6.0E-07	9.0E-07	1.2E-06	1.5E-06	1.5E-06
200	0	0	0	3.4E-09	2.8E-08	1.6E-07	3.7E-07	5.6E-07	8.3E-07	1.1E-06	1.4E-06
300	0	0	0	1.0E-09	1.0E-08	7.0E-08	2.0E-07	3.0E-07	5.0E-07	7.0E-07	1.1E-06
400	0	0	0	4.2E-10	3.5E-09	2.5E-08	8.6E-08	1.5E-07	2.5E-07	3.9E-07	5.8E-07
500	0	0	0	1.7E-10	1.5E-09	1.0E-08	4.0E-08	8.0E-08	1.3E-07	2.0E-07	3.0E-07
700	0	0	0	3.7E-11	3.1E-10	1.9E-09	8.4E-09	1.6E-08	3.0E-08	5.6E-08	1.0E-07
850	0	0	0	2.3E-11	1.1E-10	8.0E-10	3.0E-09	6.0E-09	1.0E-08	2.0E-08	4.0E-08
1000	0	0	0	1.8E-11	6.5E-11	3.1E-10	1.3E-09	1.9E-09	3.6E-09	7.0E-09	1.4E-08

Table 3

Mean atmospheric production (in $\text{in}/\text{cm}^2/\text{s}$) of cosmogenic nuclides ^7Be (block A) computed using CRAC:7Be model (Usoskin and Kovaltsov, 2008), and ^{22}Na (block B) computed here, along with their ratio (block C). The values are calculated for polar and global atmosphere where troposphere and stratosphere treated separately. The values are computed for the minimum, maximum and medium states of solar activity.

Solar activity	All ^a	Polar Tropo	Strato	All ^a	Global Tropo	Strato
<i>Block A: ^7Be production</i>						
Minimum	0.208	0.026	0.182	0.082	0.025	0.057
Medium	0.139	0.020	0.119	0.062	0.021	0.041
Maximum	0.102	0.016	0.087	0.051	0.018	0.032
<i>Block B: ^{22}Na production</i>						
Minimum	1.57E-04	1.12E-05	1.46E-04	6.47E-05	1.42E-05	5.05E-05
Medium	1.09E-04	8.86E-06	9.96E-05	5.01E-05	1.24E-05	3.78E-05
Maximum	8.12E-05	7.26E-06	7.40E-05	4.09E-05	1.09E-05	3.00E-05
<i>Block C: $^7\text{Be}/^{22}\text{Na}$ production ratio</i>						
Minimum	1324	2298	1249	1265	1734	1133
Medium	1278	2203	1196	1244	1697	1095
Maximum	1257	2142	1170	1235	1673	1076

^a Sum of troposphere and stratosphere.

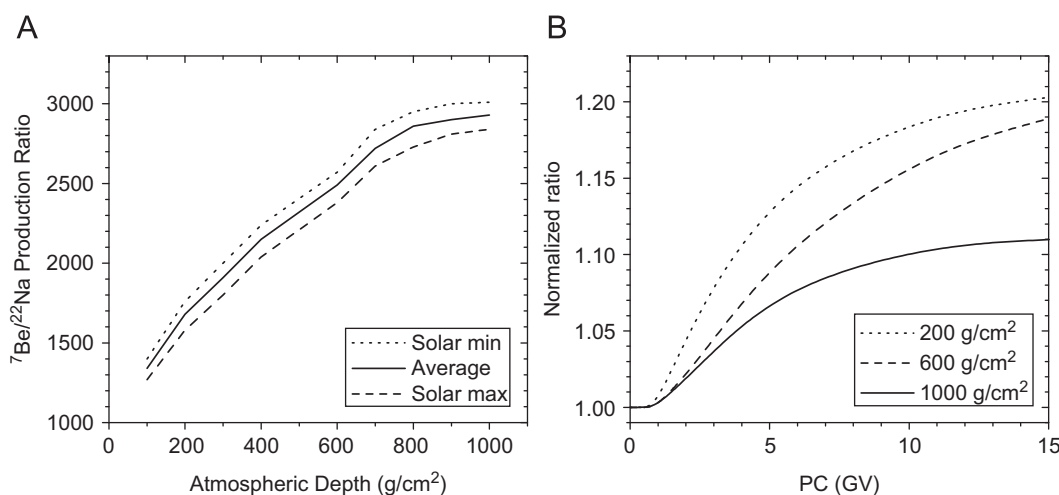


Fig. 2. Ratio of production rates of ^7Be and ^{22}Na isotopes. Panel A shows the ratio in the polar region (geomagnetic cutoff rigidity $P_c=0$) as a function of the atmospheric depth for the three levels of solar activity. Panel B shows the normalized ratio as a function of the geomagnetic cutoff rigidity for three atmospheric depths and medium solar activity level.

particles of the cascade are quite numerous but their energy is not high enough to lead to the spallation of argon to produce ^{22}Na ; nevertheless, it is still sufficient to produce ^7Be .

2.2. Estimate of the residence time

Here we present a simple estimate of the residence time of the isotopes ^7Be and ^{22}Na in the troposphere. Not aiming for detailed modeling of the atmospheric transport (cf., e.g. Jasiulionis and Wershofen, 2005; Heikkilä et al., 2009; Usoskin et al., 2009), we perform simple calculations in order to check the validity of the model computation. Let us consider a basic 2-box (stratosphere and troposphere) model of production and sink of the two isotopes. We assume a quasi-stationary case (all time derivatives are equal to zero), since the characteristic time of solar activity (viz. production) changes is large compared to other characteristic times (decay and sedimentation). For each isotope we can assume that the columnar density (in atoms per cm^2) in the stratosphere N_S is defined as

$$\frac{dN_S}{dt} = Q_S - \lambda_{\text{dec}}N_S - \lambda_{\text{TS}}N_S = 0, \quad (3)$$

where Q_S is the production term (see Table 3), $\lambda_{\text{dec}} = 1/\tau_{\text{dec}}$ corresponds to the radioactive decay life time, and $\lambda_{\text{TS}} = 1/\tau_{\text{TS}}$

corresponds to the residence time in the mean stratosphere. A similar equation can be written for the troposphere

$$\frac{dN_T}{dt} = Q_T + \lambda_{\text{TS}}N_S - \lambda_{\text{dec}}N_T - \lambda_{\text{T}}N_T = 0, \quad (4)$$

where $\lambda_{\text{T}} = 1/\tau_{\text{T}}$ corresponds to the tropospheric residence time. We note that the activity measured at the ground level does not necessarily represent the mean tropospheric concentration. According to model simulations of the vertical diffusion (Jasiulionis and Wershofen, 2005; Simon et al., 2009), the mean tropospheric concentration of the isotope is roughly five-fold of that near the ground. Thus, an estimate for that is $N_T \approx 5 \cdot n_G \cdot h_T$, where $h_T = 700 \text{ g}/\text{cm}^2$ is the tropospheric thickness, and n_G is the concentration of the isotope atoms (per gram of air) measured near the ground.

For our estimate we considered the following values. The stratospheric residence time was taken as $\tau_{\text{TS}} = 230$ days (Heikkilä et al., 2009) which corresponds to the sedimentation of the isotope carrying aerosols from the stratosphere to the troposphere. Production values have been taken from Table 3 for the polar tropospheric and global stratospheric production. For the measured isotope activities in surface air, we considered the mean values, viz. 2000 and $0.3 \mu\text{Bq}/\text{m}^3$ for ^7Be and ^{22}Na , respectively (see Section 5.1). The corresponding mean tropospheric

columnar activity appears then as $n_G \approx 3.9 \times 10^4$ and 94 at/cm² for ⁷Be and ²²Na, respectively. Finally, this oversimplified estimate of the mean tropospheric residence time yields $\tau_T = 25$ and 26 days, for ⁷Be and ²²Na, respectively. We note that the two values, calculated totally independently, are nearly equal to each other and very close to the estimate obtained using a full 3D general circulation model (GCM) (Heikkilä et al., 2009). Thus, we can conclude that our computation provides a good basis for further quantitative analysis.

3. Data collection

3.1. Aerosol sample collection

The Radiation and Nuclear Safety Authority (STUK) maintains and operates an aerosol sampler network of eight stations in Finland. This monitoring network was constructed in steps after the 1986 Chernobyl accident. This study used data from four airborne radioactivity monitoring stations of Kotka, Kajaani, Rovaniemi and Ivalo. The ⁷Be and ²²Na data covered the time period from the start of sampling until the end of July 2011, the longest time series being some 24 years from the Rovaniemi station. All stations collect aerosol samples on a weekly basis. High volume JL-900 'Snow White' aerosol samplers are located at Kotka, Kajaani and Rovaniemi. Snow White has a sampling rate of 900 m³/h (Medici, 2001). The most northern station, located at Ivalo, has a smaller sampler the JL-150 'Hunter' with a sampling rate of 150 m³/h. The sampling frequencies, volumes, sampler types and measurement times have changed over time, affecting on the detection of ²²Na. Table 4 shows information about sampling stations, whereas Fig. 3 shows their locations on a map of Scandinavia.

Aerosol particles were collected onto fibreglass filters (Whatman GF/A) 46 × 57 cm² and 27.4 × 27 cm² in size for Snow White and Hunter, respectively. The filters have a high retention capacity of over 98% even for accumulation mode aerosol particles (Mattsson et al., 1965). The nominal sampling interval was 1 week, although for a small number of samples it was up to 3 weeks. During 2007–2008, the Rovaniemi station contributed to the International Polar Year (IPY 2007–2009) by collecting and measuring daily samples. During this period there are no ²²Na observations from the Rovaniemi station. A typical sample volume for a weekly sample varied from 95,000–110,000 m³ of air. The results are commonly expressed in volumetric activity concentration (Bq/m³) which will be denoted as 'activity' in the text onwards. The sample volume information was taken directly from the air flow meter attached to the sampler. The sample volume was not normalized to standard conditions. According to Senya PLC, the manufacturer of the Snow White and Hunter samplers, the uncertainty of the sample volume is ± 2.5%.

Table 4

Data sets used in this study: ⁷Be and ²²Na activity concentrations measured in near surface air in Southern and Northern Finland.

Station	Location	Elevation (m)	Sampling time	Sample volume (10 ³ m ³)	Sampling frequency (samples/month)
Kotka	60.48°N, 26.92° E	10	1993–2011	95–190	2–4
Kajaani	64.08°N, 27.71° E	250	1999–2011	95–130	3–4
Rovaniemi	66.51°N, 25.73° E	159	1987–2011	95–110	4
Ivalo	68.64°N, 27.57° E	129	1989–2011	23–25	3–4

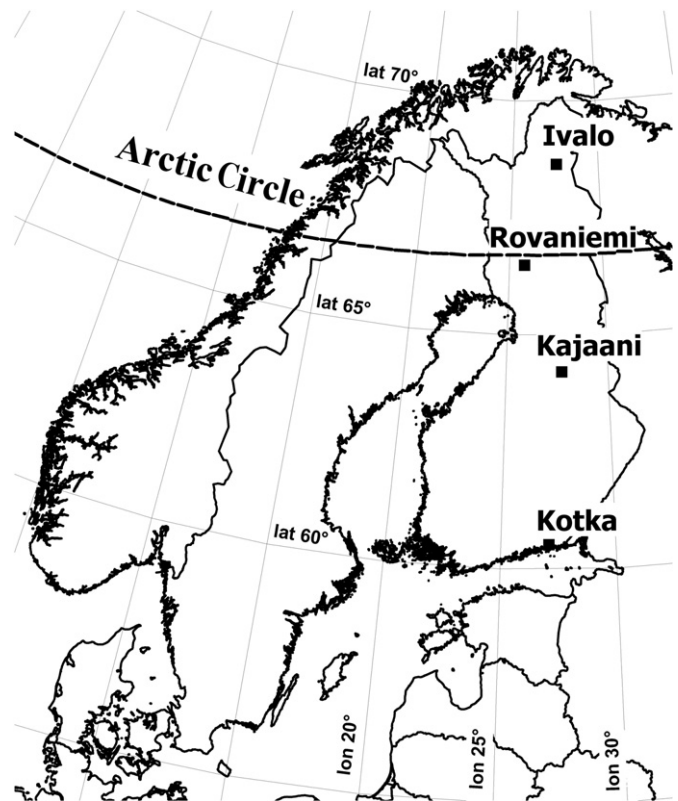


Fig. 3. Location of Finnish aerosol sampling stations used in this study.

3.2. Sample measurement

The samples were measured at Radiation and Nuclear Safety Authority's STUK laboratory which is accredited by the Finnish Accreditation Service. The laboratory meets the requirements laid down in standard EN ISO/IEC 17025:2005. Before measurement, the filters were crushed, homogenized and compressed into a 'puck' of 42 mm × 10 mm² in size and placed inside a plastic jar. The jar was placed on top of the detector and measured for γ -emitting radionuclides with a HPGe detector of 30–100% in relative efficiency. ⁷Be and ²²Na have characteristic γ -ray energy at 477 keV and at 1275 keV, respectively. The detector was mounted inside a six-inch-thick lead shield to reduce ambient background radiation. Measurement times have varied over the years from 2 to 70 h. In recent years typically 65–70 h have been used in order to detect ²²Na efficiently. Typically, the relative 1 σ statistical uncertainty for ⁷Be was 2–5% while the ²²Na uncertainty varied between 5–20% for 'high' activity samples and 20–50% for 'low' activity samples. Analysis software was used to analyze the activities of ⁷Be and ²²Na in the sample. The analysis software accepted peaks where peak significance was 70% of the Currie critical limit which leads to high relative uncertainties in the case of low activity samples. This study considered the ⁷Be and ²²Na activity data from the beginning of the monitoring until the end of July 2011. Fig. 4 shows the full time series of weekly data of ⁷Be and ²²Na activities from Kotka, Kajaani, Rovaniemi and Ivalo monitoring stations. A clear annual variation in all of the time series can be seen.

4. Data and analysis methods

The CWT can be regarded as localization in the time and frequency domains. We apply a continuous wavelet transform

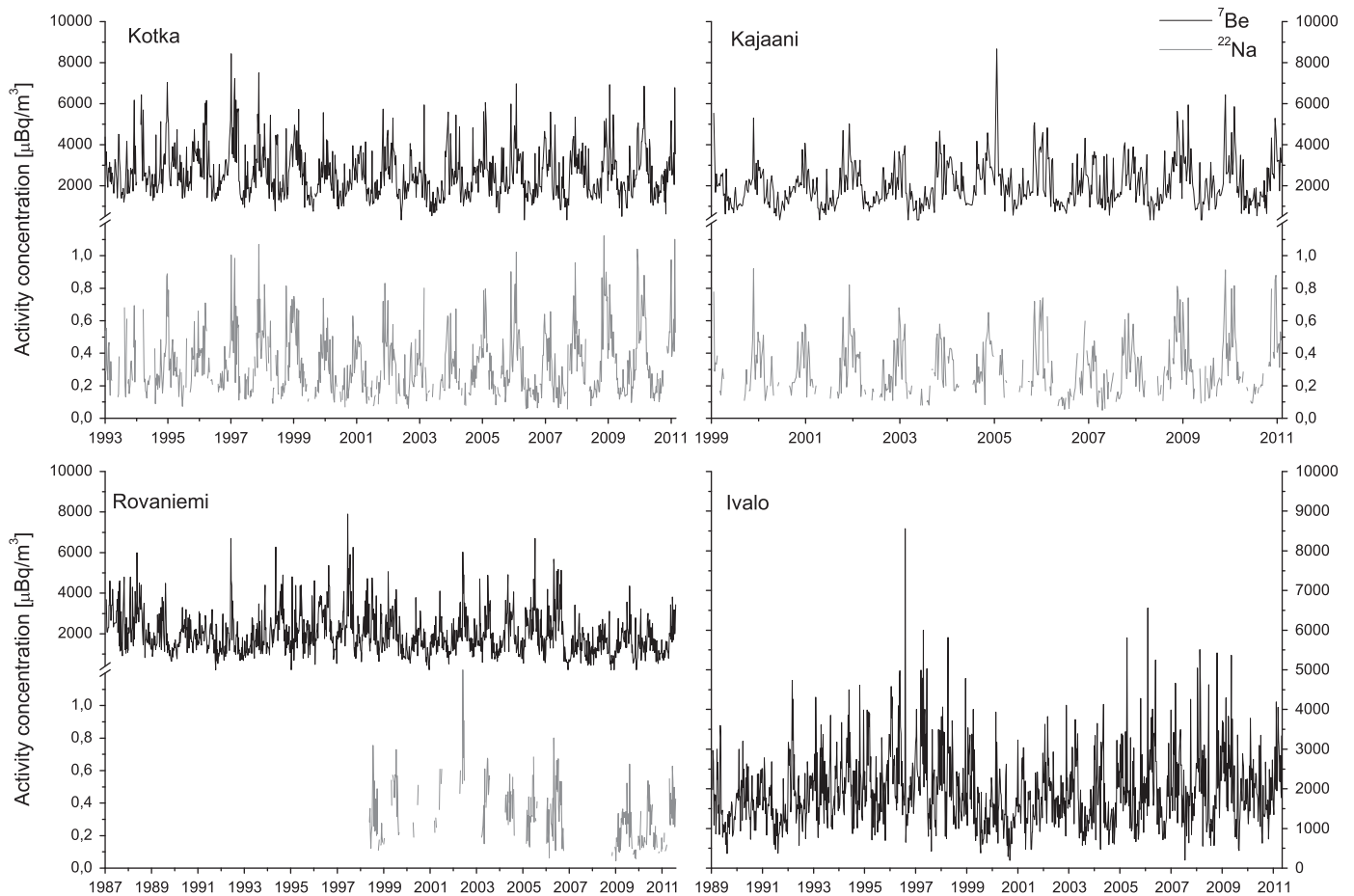


Fig. 4. Time series of ${}^7\text{Be}$ and ${}^{22}\text{Na}$ activities at near ground level with weekly sampling interval. The activity concentrations were observed at Kotka (top left), Kajaani (top right), Rovaniemi (bottom left) and Ivalo (bottom right) airborne radioactivity monitoring stations. For the CWT and coherence analyses monthly averages of the ${}^7\text{Be}$ and ${}^{22}\text{Na}$ activities were used. ${}^7\text{Be}$ data are shown in black and ${}^{22}\text{Na}$ is shown in gray color.

(CWT) using the standard Morlet basis for the wavelet spectra with the dimensionless time parameter $\omega_0 = 5$. This provides a good balance between the time and frequency localization. For the selected parameters, the time scale (i.e. effective expansion of a wavelet package in the time domain) is close to the nominal Fourier period ($\lambda = 1.03$ s). The CWT of a time series can be written as

$$W_n^X(s) = \sqrt{\frac{\delta t}{s}} \sum_{n'=1}^N x_{n'} \psi_0 \left[(n' - n) \frac{\delta t}{s} \right], \quad (5)$$

where δt is the constant time step, s is the varying scale, ψ_0 is the wavelet function.

The coherence between two data sets can be tested with the wavelet coherence analysis (WCA) method (Torrence and Compo, 1998; Grinsted et al., 2004). Wavelet coherence can be thought of as a localized correlation coefficient in time frequency space. The wavelet coherence can be defined as

$$R_n^2(s) = \frac{|S(s^{-1} W_n^{XY}(s))|^2}{S(s^{-1} |W_n^X(s)|^2) \cdot S(s^{-1} |W_n^Y(s)|^2)}, \quad (6)$$

where S is the smoothing operator and s is the circular standard deviation.

The results of the coherence analysis need to be tested before their reliability can be determined. Many geophysical time series have distinctive red noise characteristics that can be modeled by the first order autoregressive process (AR1). Since the time series

have finite lengths and CWT creates edge artefacts at the beginning and at the end of the wavelet power spectrum, the cone of influence (COI) shows the area in which the wavelet power has dropped to e^{-2} of the value at the edge due to discontinuity at the edge. In Figs. 6–11 the COI is depicted as a U-shaped cone. The dark contours indicate areas where the level of significance is above 5% against the red noise. The analysis methods were adopted from Grinsted et al. (2004) and the software package downloaded from <http://www.pol.ac.uk/home/research/waveletcoherence/>.

5. Results and discussion

5.1. Data statistics

Statistics of data from different sampling stations were compared by using a fixed time period to prevent bias in the results. In the case of ${}^7\text{Be}$, the time period of July 1999–July 2011 was used, which was determined by the shortest ${}^7\text{Be}$ data set (Kajaani). The case of ${}^{22}\text{Na}$ is more complex since ${}^{22}\text{Na}$ is not observed as frequently as ${}^7\text{Be}$ (see Fig. 4). For this comparison, the time periods of 2005–2006 and January 2009–July 2011 were selected due to sparse ${}^{22}\text{Na}$ observations at Rovaniemi. The median ${}^7\text{Be}/{}^{22}\text{Na}$ ratio values for each station are calculated using observed ${}^7\text{Be}$ and ${}^{22}\text{Na}$ values from 2005 to 2006 and from 2009 to 2011. Statistics of the data sets are presented in Table 5. The observed ${}^7\text{Be}$ and ${}^{22}\text{Na}$ median values of 1600–2400 $\mu\text{Bq}/\text{m}^3$ and

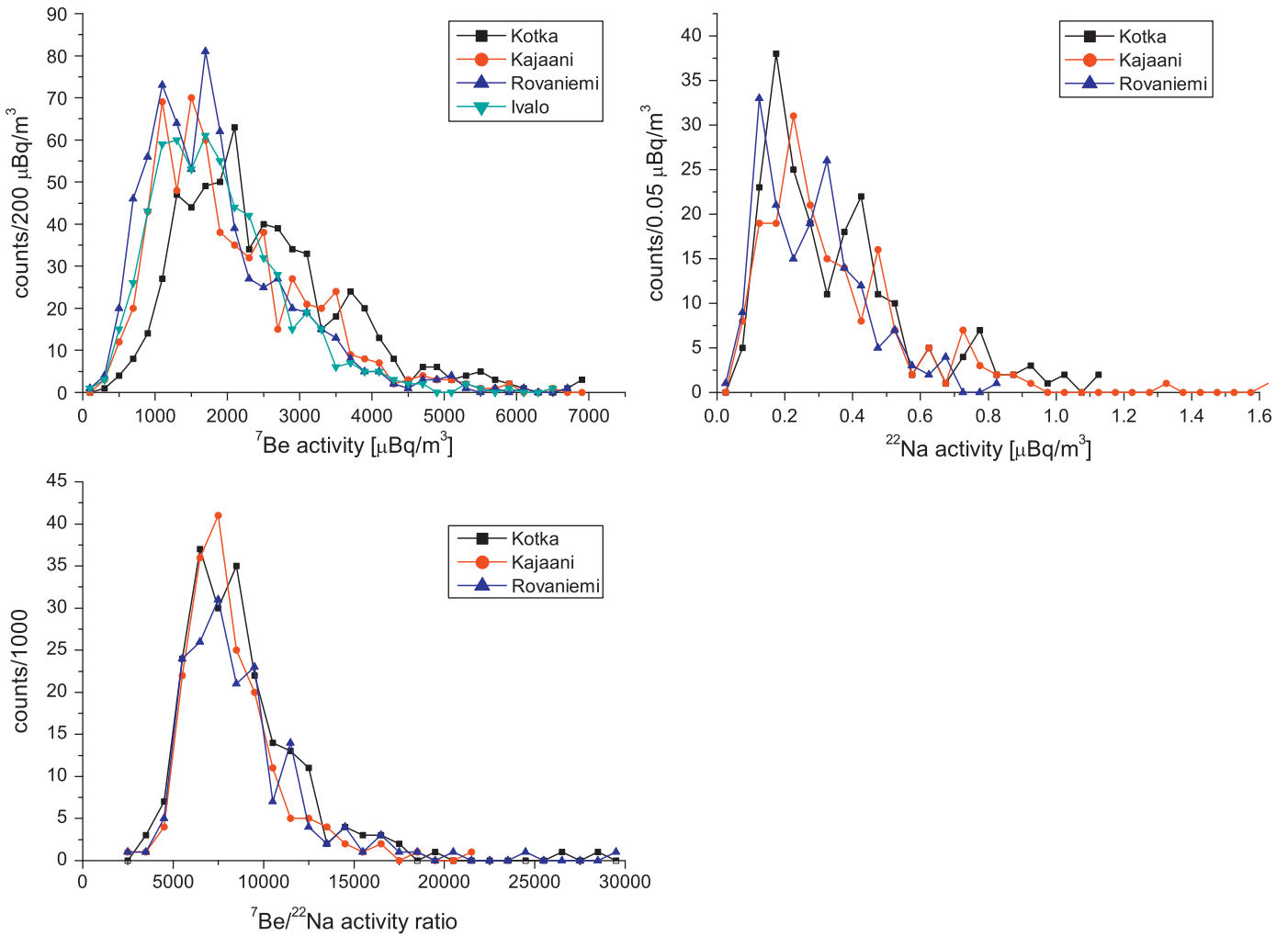


Fig. 5. Histograms of the ^7Be , ^{22}Na and $^7\text{Be}/^{22}\text{Na}$ activities. Histograms show asymmetric and lognormal distributions of ^7Be and ^{22}Na activities and $^7\text{Be}/^{22}\text{Na}$ ratio.

0.28–0.35 $\mu\text{Bq}/\text{m}^3$ are in agreement with previously reported values (e.g. Grabowska et al., 2003; Kulan et al., 2006; Rulík et al., 2009).

The median ^7Be and ^{22}Na activities show a decreasing trend with increasing latitude which agrees with the study of Kulan et al. (2006). Fig. 5 shows histograms of the observed ^7Be and ^{22}Na activities. The ^7Be and ^{22}Na data are both asymmetric and log-normally distributed. Paatero and Hatakka (2000) reported lognormal distribution of ^7Be and ^{210}Pb with median values of 2 500 and 160 $\mu\text{Bq}/\text{m}^3$ at Sodankylä in Northern Finland during 1995–1997. The statistics of the data sets are presented in Table 5. The $^7\text{Be}/^{22}\text{Na}$ ratios show similar shapes and median values for all four stations. This indicates that, in contrast to the ^7Be and ^{22}Na activities, no latitudinal dependence was observed in the $^7\text{Be}/^{22}\text{Na}$ ratio.

5.2. Interannual periodicities

Continuous equispaced time series are required for the CWT and WCA. Unfortunately, the time series shown in Fig. 4 contain gaps and the missing data were estimated to fill the gaps. In the case of ^7Be time series, there were only a few cases per station where data were missing. In these cases the gaps were filled by interpolating between adjacent data points. The missing ^{22}Na data were more complex since a larger amount of data were missing. In the Kotka ^{22}Na time series the missing data were estimated by using values of adjacent weeks and also by using the

corresponding ^7Be trend as a guideline. Since cosmogenic nuclides behave according to their carrier aerosols and are thus subjected to e.g. scavenging in a similar manner, the ^7Be trend should give a rough estimation of the ^{22}Na trend. In the Kotka ^{22}Na time series the missing data correspond to approximately 10% of the total ^{22}Na data, while in Kajaani about 27% of ^{22}Na data were missing, which is too much for estimation so no CWT or WCA was done to the Kajaani ^{22}Na data.

The CWT was used to find interannual periodicities in the ^7Be , ^{22}Na and $^7\text{Be}/^{22}\text{Na}$ time series. Interannual variability consists of periodicities longer than a year but shorter than a decade. In order to improve the CWT analysis results, the ^7Be and ^{22}Na time series were modified. Firstly, since the oscillation in the weekly time series caused by synoptic scale weather phenomena was strong, the weekly measurement data shown in Fig. 4 were converted to monthly averages in order to reduce the noise. Second, the average monthly value was subtracted from the time series so that the data represented monthly anomalies. This way, the scale was set so that the annual period did not dwarf interannual periodicities which had weaker power. Thirdly, since the time series have finite lengths, errors would occur at the beginning and at the end of the wavelet power spectrum. The beginning and the end of the ^7Be and ^{22}Na time series were padded with zeroes to bring the total length of the time series to the next power of two (Torrence and Compo, 1998). Fourthly, the probability density function of the time series was normalized before the CWT since many statistical tests assume a normal distribution of

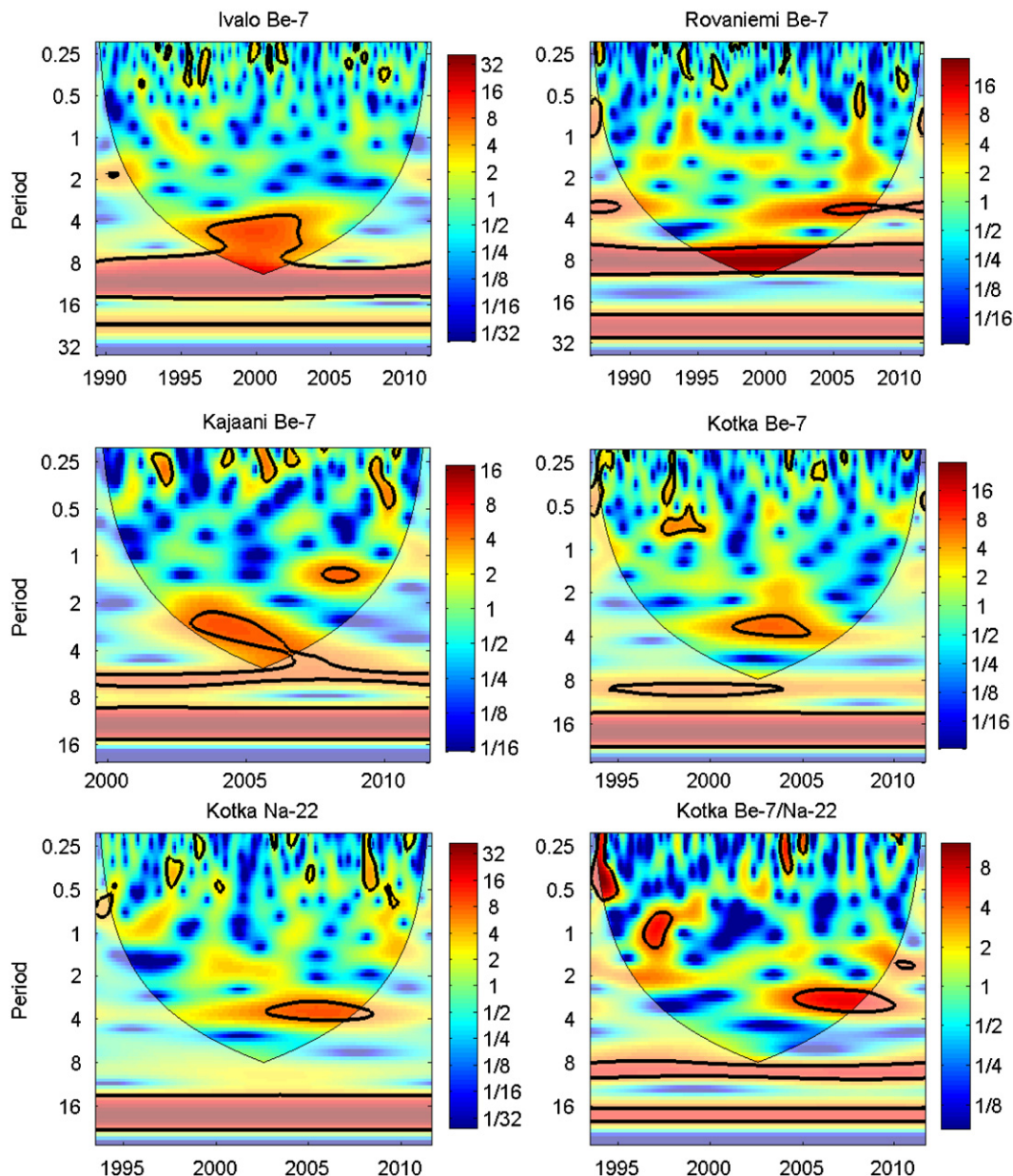


Fig. 6. CWT analyses of the cosmogenic ^7Be and ^{22}Na time series. Periodicities above a 5% significance level against red noise are depicted by dark contours. The cone of influence is shown in a lighter shade. The bars and scales on the right side of the plots show the wavelet power. (For interpretation of the references to color in this figure legend, the reader is referred to the web version of this article.)

the probability density function (Grinsted et al., 2004). As it was shown in Fig. 5, the ^7Be and ^{22}Na activities were log-normally distributed.

Fig. 6 shows the CWT analyses of the modified ^7Be , ^{22}Na and $^7\text{Be}/^{22}\text{Na}$ time series. In the figure, the x -axis represents time and the y -axis period, where the unit is 1 year. The areas above 5% significance level against red noise are depicted by dark contours. If a strong and stable periodicity is present throughout the time series then a continuous band at a certain period is seen. In the case of intermittent periodicity, where power fluctuates above and below the noise level, 'islands' of periodicity are created.

The CWT analyses show different sets of periodicities for each data set. In the Ivalo ^7Be data, the CWT analysis finds periodicities at the 4–8 year scale. The Rovaniemi ^7Be data show periodicity at 2.5–3.5 and 8 year scales. In each of the Kotka data sets only one periodicity 'island' at 2–3.5 year scale was observed. In Kajaani data an 'island' was also seen at the 2–3.5 year scale.

The 2.5–3.5 year periodicity has a wavelet power around 6. This period was found in Kotka, Kajaani and Rovaniemi data sets and it was observed to be intermittent. In the Ivalo data, this periodicity was not observed. The period of 2.5–3.5 years was present in all three data sets although the temporal location seemed to vary during 2003–2007. The weakest power of this periodicity was seen in Rovaniemi. Similar to the 2.5–3.5 year periodicity, the 4–6 year periodicity was also observed to be intermittent. This periodicity had a wavelet power also around 6 and the periodicity was only seen in the northernmost ^7Be data from Ivalo where it was present between 1996 and 2003. The periodicity at the 7–8 year scale was stronger and more stable than periods discussed above. This period is represented by a band in Fig. 6. The 7–8 year periodicity had wavelet power around 20, roughly three times higher than the 2.5–3.5 and 4–6 year periodicities. In the Ivalo and Rovaniemi data the 7–8 year periodicity is clear. In the case of the Kotka ^7Be and $^7\text{Be}/^{22}\text{Na}$ data, the tip of the COI touches the

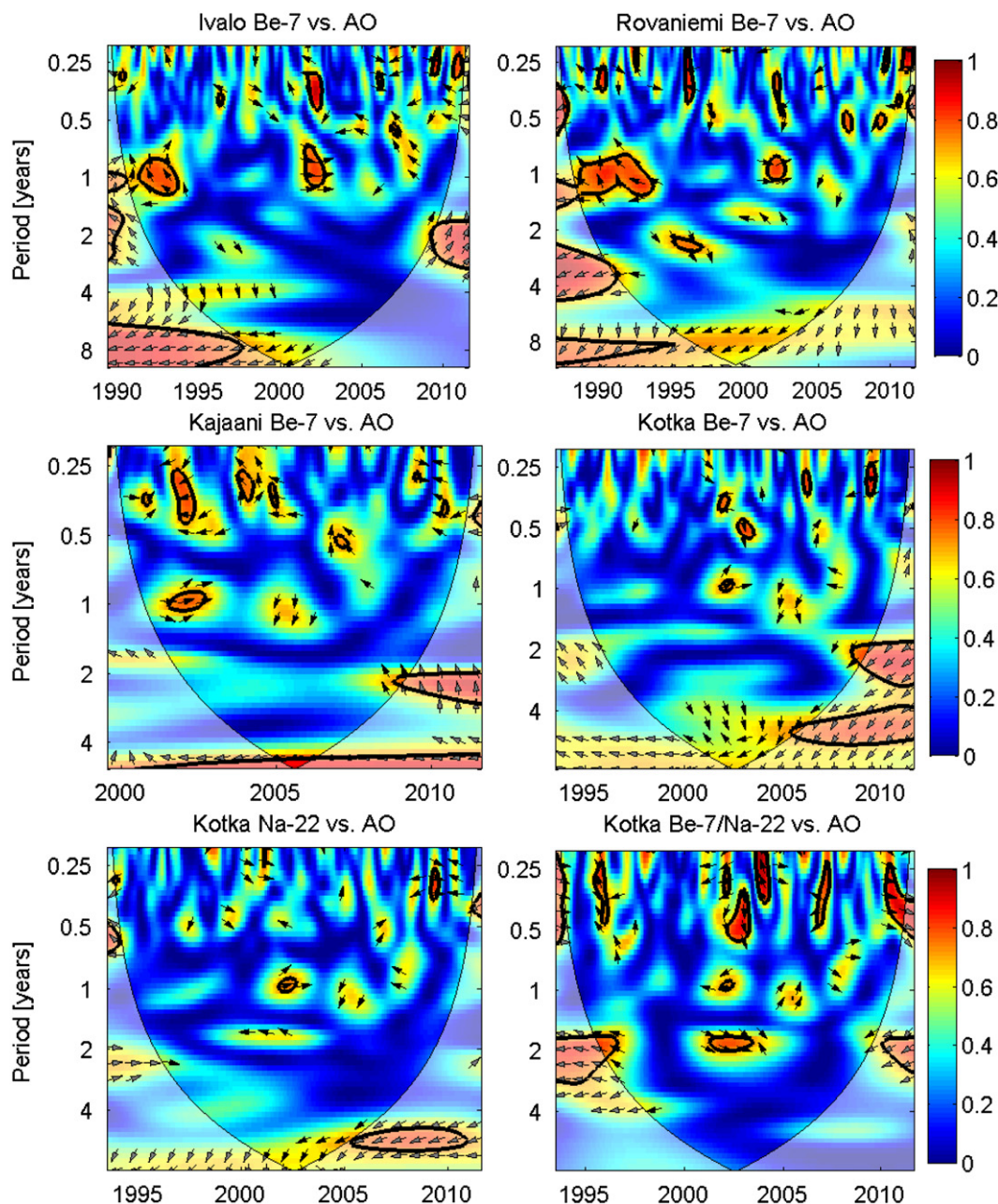


Fig. 7. WCA of the ^7Be and ^{22}Na time series and Arctic Oscillation (AO) index. Dark contours indicate significant areas above a 5% significance level against red noise. The colored bars on the right show the strength of correlation. Arrows indicate the phase difference. (For interpretation of the references to color in this figure legend, the reader is referred to the web version of this article.)

7–8 year band. The band is outside the COI but with certain confidence we assume that 7–8 year periodicity was present in those time series. Each studied data set showed a unique set of periodicities, which is in agreement with the previous findings (Leppänen et al., 2010). Table 6 shows the interannual periodicities found in CWT analyses of ^7Be , ^{22}Na and $^7\text{Be}/^{22}\text{Na}$ data sets.

The periodicities located outside the COI should be considered as possible artefacts from edge effects. The lengths of the time series used in this study are too short to reliably analyze interdecadal periodicities. Several authors have reported the influence of the 11-year solar cycle to ^7Be activities at ground level, see e.g. Talpos et al. (2005) and Hedfors et al. (2006). It should be noted that solar modulation affects ground level ^7Be activities in Southern Finland, but not in Northern Finland. The influence of solar modulation on ambient air ^7Be activity in Sweden and Finland has been previously

discussed in Leppänen et al. (2010). In Fig. 6, outside the COI, there are indications of periodicities represented by bands around the 14–16 and 20–22 year scales. Both the 14–16 and 20–25 year periodicities are well studied and can be found in different data series, e.g. in surface and sea surface temperatures, precipitation periodicities, tree rings and in ^{10}Be time series (Raspopov et al., 2004; Kasatkina et al., 2007; Velasco and Mendoza, 2008; Partal, 2010). The 13.9 year periodicity has been attributed to propagation of ENSO signal from the western Pacific eastwards up to the polar regions (Jevrejeva et al., 2007). The decadal periodicities are thought to be a result of the influence of the solar Hale cycle on climatic parameters. It was thought that these periods are generated by real physical phenomena and one can expect to find these periodicities in the time series in the future when enough data have been gathered to make the time series long enough for the CWT.

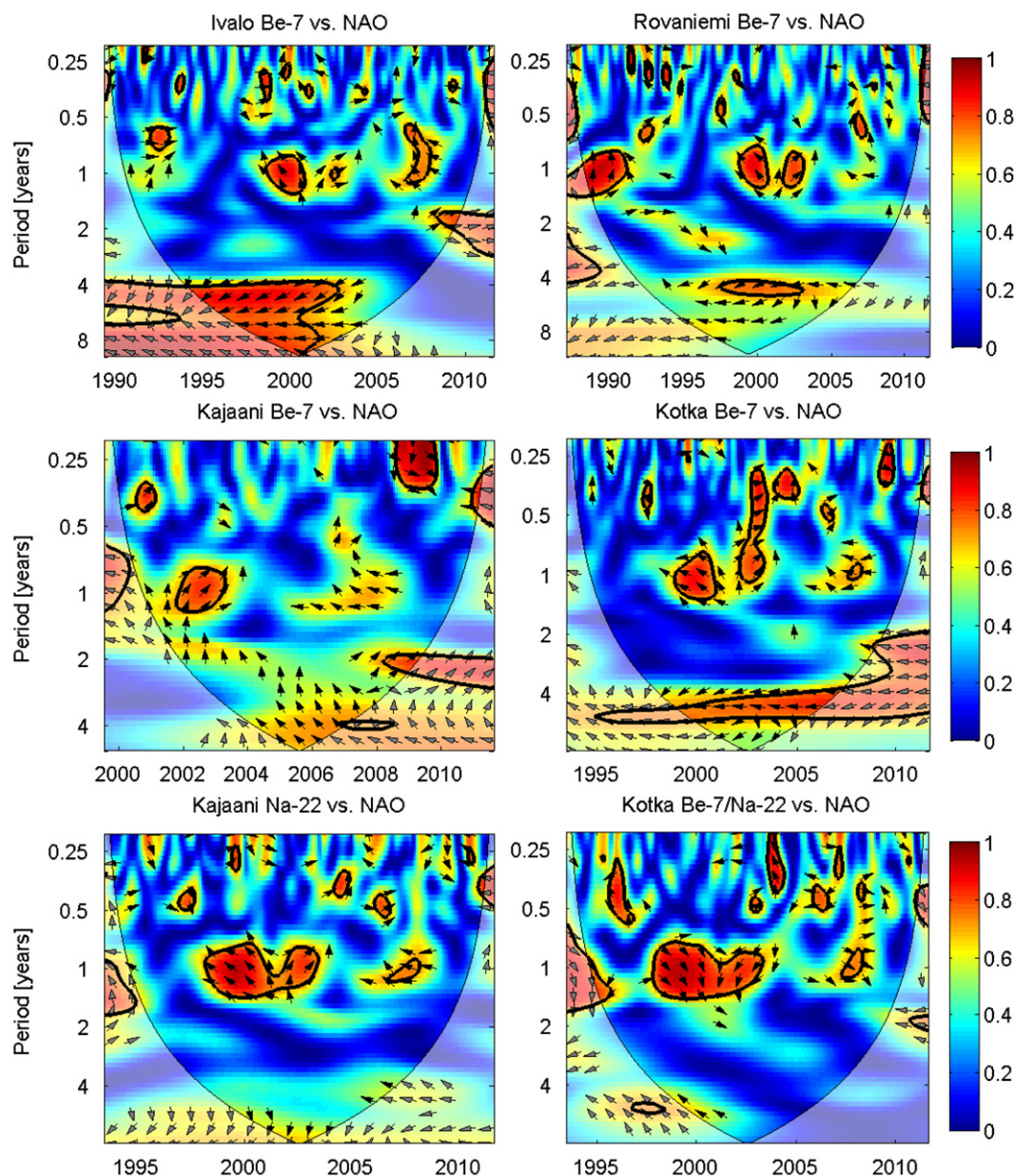


Fig. 8. Wavelet coherence analysis of the ^7Be and ^{22}Na time series and North Atlantic Oscillation (NAO) index. Dark contours indicate significant areas above a 5% significance level against red noise. The colored bar on the right side show the strength of correlation. Arrows indicate the phase difference. (For interpretation of the references to color in this figure legend, the reader is referred to the web version of this article.)

5.3. ^7Be and ^{22}Na coherence with climatic phenomena

The wavelet coherence analysis (WCA) was applied to study coherence between average monthly ^7Be and ^{22}Na activity data and different climatic indices and find causes for periodicities found in the CWT analyses in Section 5.2. This was done by searching phase-locked coherence between the ^7Be and ^{22}Na data sets and an index at a characteristic period. A real coherence is indicated as bands or as islands inside dark contours when the arrows indicating phase difference are all pointing in the same direction. Random coherences typically have varying phases where arrows indicating phase difference are not consistently pointing in one direction or random coherence is intermittent which can be a coincidence of two independent variable signals with a similar period.

For the WCA, 15,000 surrogate AR1 red noise data set pairs were created to test the significance of the coherence. The arrows

in Figs. 7–11 indicate the relative phase shift of the two time series. Arrows pointing to the right indicate the series are in-phase, arrows pointing to the left indicate the series are in anti-phase, arrows pointing down series 1 leads series 2 by 90° , and arrows pointing up series 2 leads series 1 by 90° (Grinsted et al., 2004).

The monthly index data for AO, NAO, QBO, SO and AMO were obtained from the National Oceanic and Atmospheric Administration (NOAA) websites at <http://www.cpc.noaa.gov/> and at <http://www.esrl.noaa.gov/psd/data/timeseries/AMO/>.

5.3.1. ^7Be and ^{22}Na coherence with Arctic Oscillation

The Arctic Oscillation (AO) can be defined as an index of the dominant pattern of non-seasonal sea-level pressure variations north of 20° N latitude. The AO is expected to show variability at 2.2–3.5, 5.7–7.8 and 12–20 year periods (Jevrejeva et al., 2003).

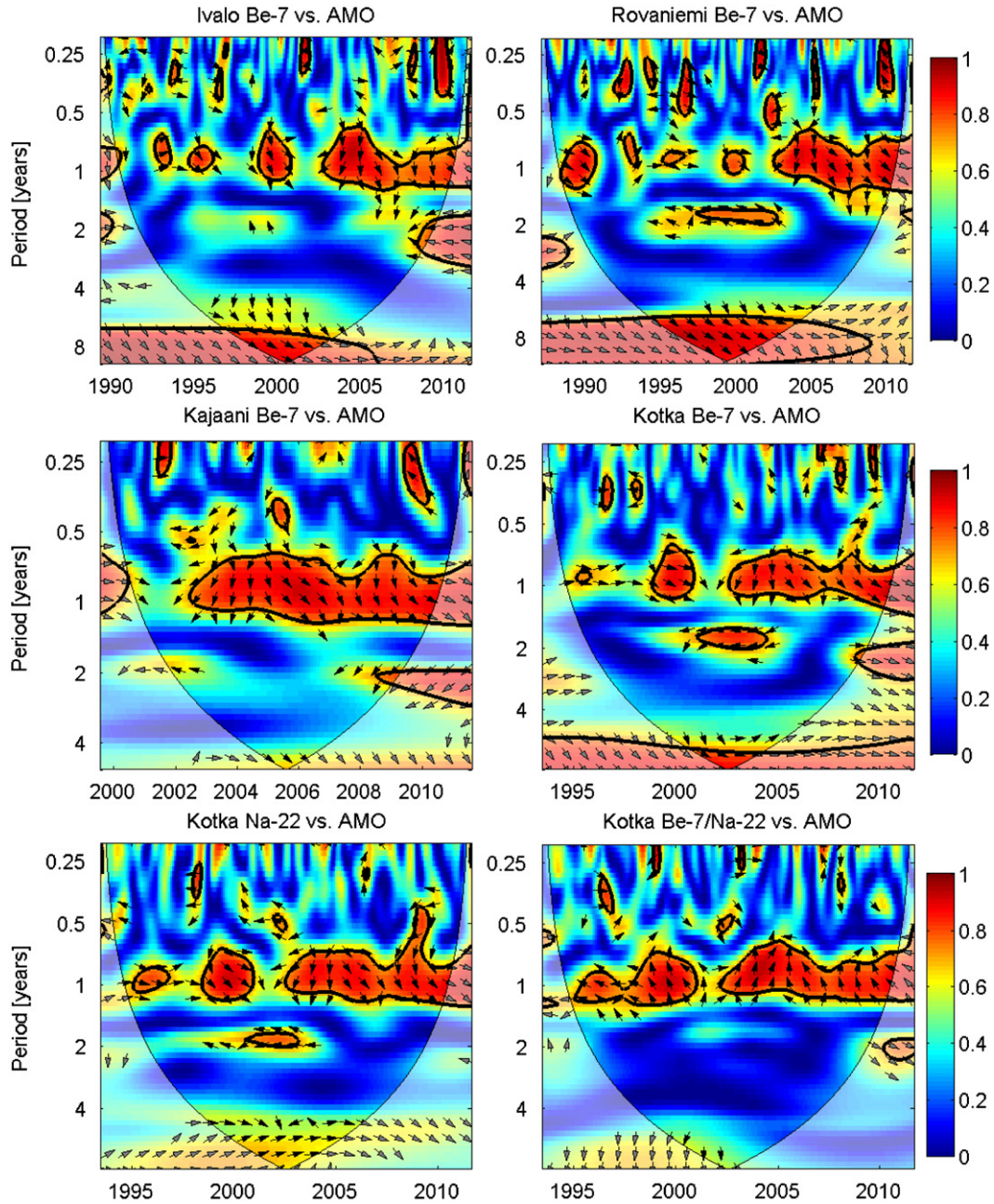


Fig. 9. Wavelet coherence analysis of the ^7Be and ^{22}Na time series and Atlantic Multidecadal Oscillation. Dark contours indicate significant areas above a 5% significance level against red noise. The colored bar on the right side show the strength of correlation. Arrows indicate the phase difference. (For interpretation of the references to color in this figure legend, the reader is referred to the web version of this article.)

Fig. 7 shows the Wavelet coherence analysis of ^7Be and ^{22}Na time series and the AO index.

In Fig. 7, no clear coherences were found with the AO index and any of the ^7Be and ^{22}Na data sets. The only case where a possible coherence could be observed was in the Kajaani ^7Be data where an anti-phase coherence was observed at ~ 6 year scale. Unfortunately, due to the shortness of the time series only the tip of the COI is inside the coherence band. It can be speculated that AO is the cause of the ~ 6 year periodicity observed in CWT analysis of Kajaani ^7Be data (see Fig. 6).

5.3.2. ^7Be and ^{22}Na coherence with North Atlantic Oscillation

The North Atlantic Oscillation (NAO) can be viewed as a subset of the AO (Jevrejeva and Moore, 2001). NAO is a periodic variation

of the temperature and salinity conditions in the North Atlantic Ocean (Rodwell et al., 1999). The NAO variations cause periodic climatic differences in e.g. air temperature, wind direction and speed distributions leading even to biological variations (Weyhenmeyer et al., 1999). The NAO index is defined as the difference in atmospheric pressure at sea level between the Icelandic low and the Azores high. The NAO presents a weak red noise spectrum with 2-weak periods at 2 years and at 8–10 year scales (Greatbatch, 2000). During 1988–1995 the AO/NAO had a strong positive phase. The results of the wavelet coherence analysis between the ^7Be and ^{22}Na data and the NAO index are shown in Fig. 8.

In the Fig. 8, clear anti-phase coherences with the NAO index and the ^7Be data can be observed at all the stations. Unlike the ^7Be data, the ^{22}Na and $^7\text{Be}/^{22}\text{Na}$ data from Kotka station did not show

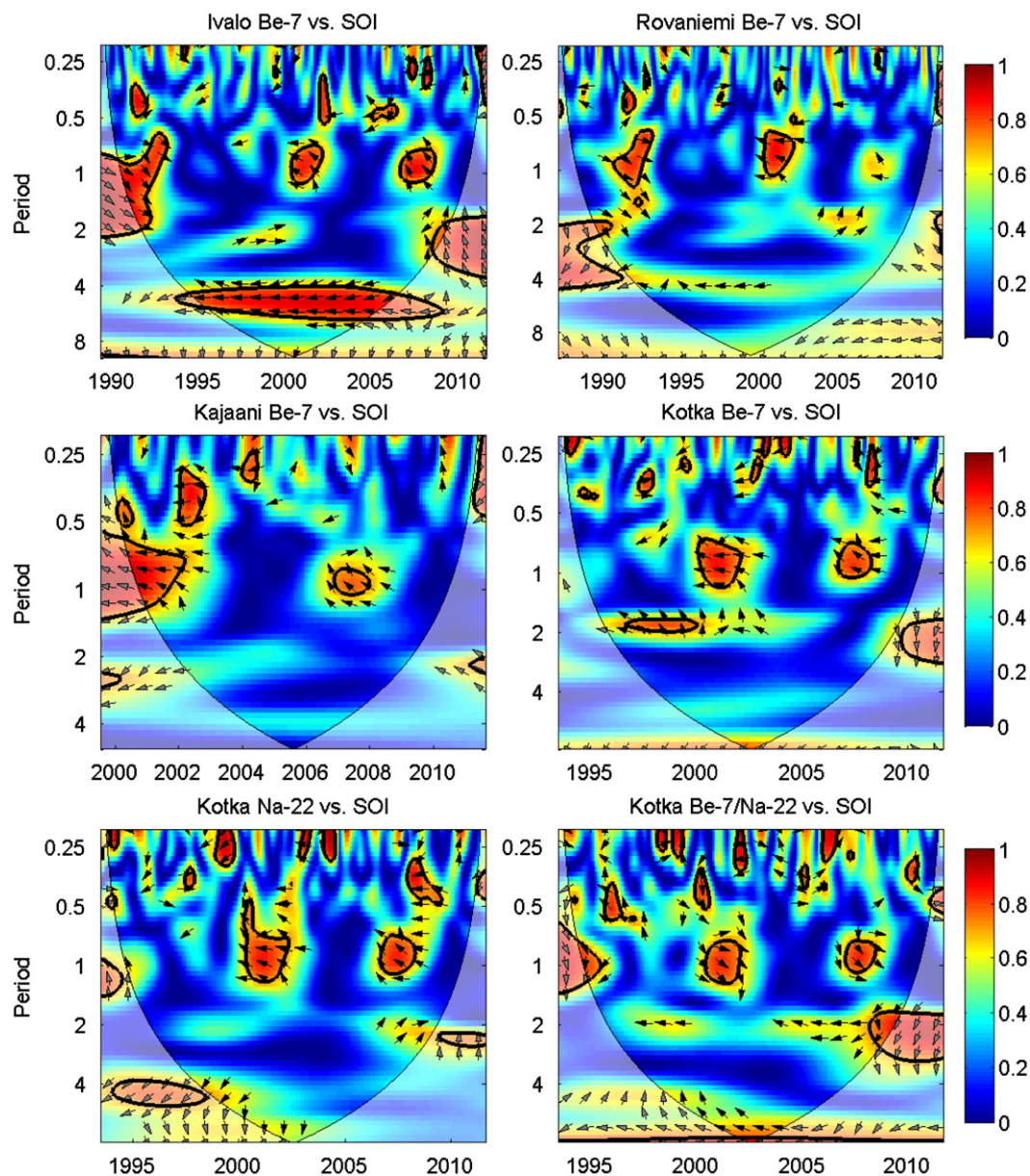


Fig. 10. Wavelet coherence analysis of the ^7Be and ^{22}Na time series and Southern Oscillation Index (SOI). Dark contours indicate significant areas above 5% significance level against red noise. The colored bar on the right side indicate the strength of correlation. Arrows indicate the phase difference. (For interpretation of the references to color in this figure legend, the reader is referred to the web version of this article.)

any coherence with the NAO index. The Ivalo ^7Be data shows anti-phase coherence at the 4–6 year scale until 2002 and at the 7–8 year scale until 2001. The Rovaniemi data show coherence at the 4–5 year scale from 1998 until 2004, while the Kotka ^7Be data show coherence at the 4–6 year scale extending through the whole time series. Table 7 shows the average phase angles found in the WCA between the ^7Be data and the NAO index. The results show anti-phase coherence in all ^7Be data sets.

These findings are in agreement with the studies of ^{10}Be concentrations in ice cores and the NAO index where coherences at multiple scales extending from 7–8 years up to 80–96 years were observed (Velasco and Mendoza, 2008). When the NAO is in its positive phase, the westerly winds become more dominant bringing maritime air masses with low ^7Be concentrations to Finland. The abundant precipitation associated with these air masses removes aerosol particles with wet deposition. Furthermore, the upward movement of air in low-pressure situations

hinders the transfer of cosmogenic radionuclides from the upper troposphere to the surface air. On the other hand, during the negative phase of NAO, Finland is affected more by continental air masses. These air masses usually have high concentrations of ^7Be . This is associated with high-pressure situations in Central Russia; and the downward motion of the air masses brings ^7Be from the upper troposphere to lower altitudes. Moreover, the moisture content of these air masses is usually low, and the lack of precipitation prevents the removal of ^7Be by wet deposition. A similar dependence between the NAO and airborne ^{210}Pb has been observed earlier by Paatero et al. (2000). Since in low altitudes aerosols are scavenged in the same manner, regardless of which cosmogenic isotope it carries, both ^7Be and ^{22}Na should show similar coherences with climatic indices; however, this was not observed. The difference between the ^7Be and ^{22}Na behavior can be understood as a difference in production altitudes. While 25% of ^7Be is being produced in the troposphere, approximately

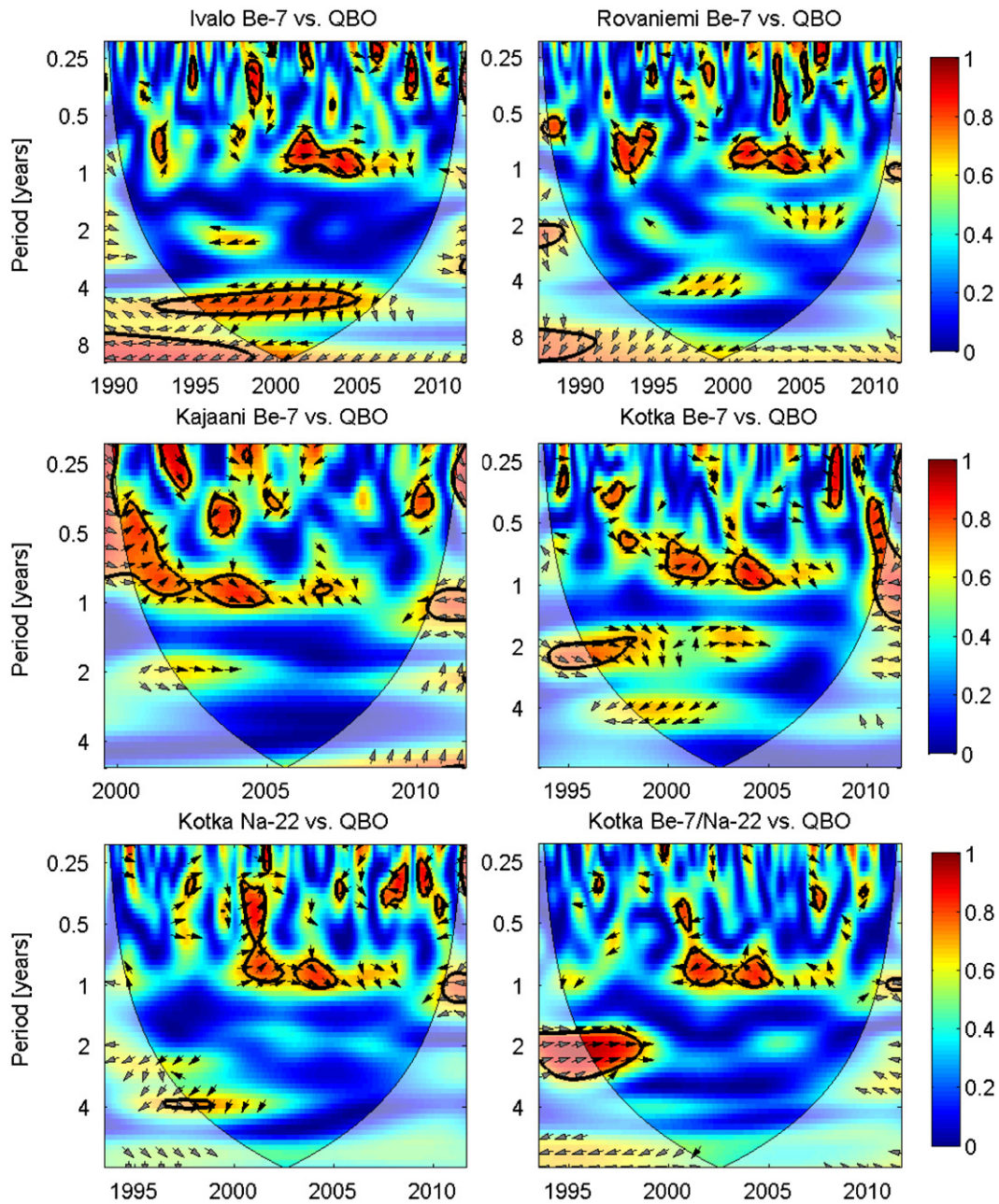


Fig. 11. Wavelet coherence analysis of the ^7Be and ^{22}Na time series and Quasi Biennial Oscillation (QBO) index. Dark contours indicate significant areas above a 5% significance level against red noise. The colored bar on the right side indicate the strength of correlation. Arrows indicate the phase difference. (For interpretation of the references to color in this figure legend, the reader is referred to the web version of this article.)

Table 5
 Statistics of ^7Be and ^{22}Na activities. The ^7Be data cover period of July 1999–July 2011 and ^{22}Na data cover years 2005–2006 and time period of January 2009–July 2011.

Location	N_{Be}	Median ^7Be ($\mu\text{Bq}/\text{m}^3$)	^7Be (min–max) ($\mu\text{Bq}/\text{m}^3$)	N_{Na}	Median ^{22}Na ($\mu\text{Bq}/\text{m}^3$)	^{22}Na (min–max) ($\mu\text{Bq}/\text{m}^3$)	Median $^7\text{Be}/^{22}\text{Na}$ ratio in activity/in number of atoms
Kotka	621	2210	270–6970	213	0.30	0.05–1.12	8100/450
Kajaani	622	1750	250–8660	183	0.28	0.05–1.63	7640/430
Rovaniemi	628	1640	190–6700	172	0.27	0.05–0.8	7950/450
Ivalo	608	1740	190–6560				

N =number of observations.

10% of the ^{22}Na is produced in the troposphere (see Table 3) where it would be subjected to different meteorological conditions compared to the stratosphere.

5.3.3. ^7Be and ^{22}Na coherence with Atlantic Multidecadal Oscillation
 The Atlantic Multidecadal Oscillation (AMO) is a mode variability occurring in the North Atlantic Ocean, with its principal

Table 6
Interannual periodicities found in the CWT analyses of ^7Be , ^{22}Na and $^7\text{Be}/^{22}\text{Na}$ data sets.

Observed period (years)	Ivalo	Rovaniemi	Kajaani	Kotka (^7Be)	Kotka (^{22}Na)	Kotka ($^7\text{Be}/^{22}\text{Na}$)	Wavelet power
2.5–3.5		X	X	X	X	X	~ 6
4–6	X		X				~ 6
7–8	X	X		x		x	~ 20

X=inside the COI; x=outside the COI.

Table 7
The average phase angles between ^7Be data and the NAO index.

Period (years)	Ivalo	Rovaniemi	Kajaani	Kotka
4–6	$155^\circ \pm 54^\circ$	$-178^\circ \pm 54^\circ$	$-142^\circ \pm 25^\circ$	$177^\circ \pm 19^\circ$
7–8	$161^\circ \pm 58^\circ$			

expression in the sea surface temperature (SST) field. The AMO instrumental record shows periodicities at 3.5, 7–10, 18–60 years (Poore et al., 2009). A relationship between an intermittent NAO cycle and the AMO signal suggests coupling of the ocean-atmosphere system at multidecadal time scales (Hubeny et al., 2006). However, the nature and origin of AMO is still uncertain (Knudsen et al., 2011). The AMO is known to modulate ^{10}Be concentrations in ice cores at multiple time scales from which the three shortest periodicities were 3–3.5, 5.5–6.5 and 11–15 years (Velasco and Mendoza, 2008).

Fig. 9 shows the results of the WCA of the ^7Be and ^{22}Na data and the AMO index. In the Kotka, Rovaniemi and Ivalo ^7Be data, a clear in-phase coherence was found at the 7–8 year time scale where the average phase angles were around 25° – 30° . This phase difference translates into a time lag of approximately 7–8 months. The in-phase coherence with the 25° – 30° phase difference would mean that ^7Be leads the AMO. It is possible that ^7Be and AMO follow a common driver and changes are first seen in ^7Be activities. However, another possibility, and a more plausible one, is a software related problem where the series are actually in anti-phase coherence with the 205° – 210° mean phase angle. The increasing AMO index means increasing sea-surface temperatures, which lead to more evaporation and increased precipitation, and thus, increasing the scavenging of atmospheric aerosols carrying cosmogenic isotopes. In the Kotka data sets, the ^7Be was in coherence with the AMO but the ^{22}Na was not. This type of behavior of ^7Be and ^{22}Na was also observed in Section 5.3.2 when coherence with NAO was studied.

5.3.4. ^7Be and ^{22}Na coherence with the southern oscillation

For this study, the atmospheric component of the El Niño-Southern Oscillation (ENSO) was selected. The Southern Oscillation Index (SOI) is defined as sea-level pressure difference between Tahiti and Darwin, Australia. The time series of the SOI and sea surface temperatures in the eastern equatorial Pacific indicate that the ENSO cycle has an average period of about 4 years, although in the historical record the period has varied between 2 and 7 years. The 1980s and 1990s featured a very active ENSO cycle, with five El Niño episodes (1982/1983, 1986/1987, 1991–1993, 1994/1995, and 1997/1998) and three La Niña episodes (1984/1985, 1988/1989, 1995/1996).

In previous studies, Velasco and Mendoza (2008) reported a coherence between ^{10}Be and the SOI at 32 and 64 year scales while (Koch and Mann, 1996) studied interannual variations in ^7Be activities from 19 locations distributed globally and found a 2–3 year period which was attributed to ENSO. In Scandinavia, Jevrejeva et al. (2003) found an anti-phase coherence between the

Table 8
Summary of the wavelet coherence analyses of the ^7Be and ^{22}Na data and different climate indices.

Period (years)	Ivalo	Rovaniemi	Kajaani	Kotka ^7Be	Kotka $^7\text{Be}/^{22}\text{Na}$
2–3				QBO	QBO
4–6	NAO, SO	NAO	AO(?)	NAO	
7–8	NAO, AMO	AMO		AMO	

Baltic maximum sea ice extent (BMI) and the SOI. The tropics is speculated to be linked to the polar vortex and to the Arctic via a stratospheric bridge (Jevrejeva et al., 2004). Fig. 10 shows the results of the WCA between ^7Be and ^{22}Na data sets and the SOI. An anti-phase coherence between the Ivalo ^7Be data and the SOI was found. This coherence can be seen at the 4–6 year scale from 1994 until 2006. The mean phase angle was $174^\circ \pm 19^\circ$. The high-latitude location of the Ivalo station is advantageous for observing changes in the Arctic circulation patterns.

5.3.5. ^7Be and ^{22}Na coherence with QBO

The Quasi-Biennial Oscillation (QBO) is defined as quasi-periodic oscillation of the equatorial zonal wind between easterlies and westerlies in the tropical stratosphere. The QBO has a mean period of 28–29 months. According to Baldwin and Dunkerton (2001) the QBO modulates extra-tropical wave propagation, thus affecting the breakdown of the wintertime stratospheric vortices. The polar vortex in the stratosphere affects surface weather patterns providing a mechanism for the QBO to have an effect on high-latitude weather patterns. In previous studies, the QBO has been found to modulate ground-level ^7Be activities in Greece (Gerasopoulos et al., 2003).

In Fig. 11 the in-phase coherence was found in the Kotka ^7Be and $^7\text{Be}/^{22}\text{Na}$ data sets. The $^7\text{Be}/^{22}\text{Na}$ data show stronger coherence than the ^7Be data, the correlation coefficients being ~ 0.9 and ~ 0.7 respectively. Both coherences were seen at the 2–3 year scale until 1999. The average phase angle between the QBO and the Kotka ^7Be data was $53^\circ \pm 58$ and between the QBO and the Kotka $^7\text{Be}/^{22}\text{Na}$ data, $-7^\circ \pm 70^\circ$. Interestingly, the WCA shows coherence in the Ivalo ^7Be data at 4–6 and at 8 year scales. These periods are not characteristic of the QBO but are characteristic of the NAO and the SO.

5.3.6. Summary of the WCA analyses

The interannual periodicities found in ^7Be and ^{22}Na time series in the CWT analyses, shown in Table 6 have been linked to different climatic phenomena in the WCA analyses. Table 8 shows the summary of the WCA results of ^7Be and ^{22}Na time series and different climate indices.

5.4. $^7\text{Be}/^{22}\text{Na}$ ratio as an atmospheric tracer

In earlier studies the $^{10}\text{Be}/^7\text{Be}$ ratio has been proposed as a radiochronometer, or tracer, for atmospheric transport processes (Raisbeck et al., 1981; Jordan et al., 2003). The beryllium isotopes

are chemically identical but ^7Be has a significantly shorter half-life than ^{10}Be ($T_{1/2}=1.36$ My). The use of the $^{10}\text{Be}/^7\text{Be}$ ratio as an atmospheric tracer is not straightforward due to the long half-life of ^{10}Be , which requires Accelerator Mass Spectroscopy (AMS) to measure its concentrations. The activities of ^7Be and ^{22}Na can be determined simultaneously in a γ -spectroscopic measurement from an aerosol filter sample. The $^7\text{Be}/^{22}\text{Na}$ activity ratio can be considered as a radiochronometer assuming that aerosols carrying different types of cosmogenic isotopes behave in a similar manner. This means that atmospheric processes, e.g. wet scavenging can change concentrations, but it should not change the $^7\text{Be}/^{22}\text{Na}$ activity ratio.

In Fig. 12, $^7\text{Be}/^{22}\text{Na}$ activity ratios are shown in the Kotka, Kajaani and Rovaniemi data sets from the beginning of January 2006 until end of July 2011. The ratios show significant variability at a synoptic scale, but at an annual level, the behavior of the time series from different stations were nearly identical. This can also be seen from the $^7\text{Be}/^{22}\text{Na}$ histogram in Fig. 5. A clear annual trend in the $^7\text{Be}/^{22}\text{Na}$ ratio can be seen where higher ratios are detected during winter and lower ratios during summer. This is opposite to the observations of the ^7Be and ^{22}Na activities, where higher activities are observed during summer and lower ones during winter (see Fig. 4). Observations of the $^7\text{Be}/^{22}\text{Na}$ ratio in this study are in accordance with the observations of the $^{10}\text{Be}/^7\text{Be}$ ratio in Sweden, where the $^{10}\text{Be}/^7\text{Be}$ ratio reached low values during winter and high values during summer (Aldahan et al., 2001). Aldahan et al. (2001) used the $^{10}\text{Be}/^7\text{Be}$ ratio, which produces a 'mirror image' compared to the $^7\text{Be}/^{22}\text{Na}$ ratio used in this study. Nonetheless, it can be concluded that the seasonal behavior of the $^7\text{Be}/^{22}\text{Na}$ and the $^{10}\text{Be}/^7\text{Be}$ ratios are similar.

In order to compare $^7\text{Be}/^{22}\text{Na}$ ratios to the calculated ones discussed in Section 2.1, the measured ^7Be and ^{22}Na activities were converted to number densities using formula (7)

$$N = \frac{A \times T_{1/2}}{\ln 2} \quad (7)$$

where N is number density (atoms/m³), A is measured activity (Bq/m³) and $T_{1/2}$ is half-life of the isotope.

In Fig. 12, the time series of the $^7\text{Be}/^{22}\text{Na}$ ratio from Rovaniemi, Kajaani and Kotka are shown from the beginning of January 2006 until the end of July 2011. The left y-axis shows the $^7\text{Be}/^{22}\text{Na}$ ratio in activity, as it is measured, while the right y-axis shows the $^7\text{Be}/^{22}\text{Na}$ ratio after converting activity into atoms with Eq. (7).

In Fig. 12, during winter months (November–March) the $^7\text{Be}/^{22}\text{Na}$ ratios show a strong oscillation in the weekly time series caused by synoptic scale weather phenomena, typically between 7000 and 11,000 in activity (or 450–700 in number of atoms). The synoptic variation was particularly large during the warm and moist winters of 2007 and 2008 when there was a strong positive NAO phase. In 2010–2011 the NAO had a strong negative phase; these winters were cold and dry in Finland. The prevailing air masses have been more steadily of continental origin, and the cyclogenesis over the North Atlantic Ocean modifying the $^7\text{Be}/^{22}\text{Na}$ activity ratio has been less active and is observed as a smaller variation in the ratio. During summer months (June–August) the $^7\text{Be}/^{22}\text{Na}$ ratios show significantly reduced short-term variation. Typical $^7\text{Be}/^{22}\text{Na}$ ratios vary between 5000 and 7000 (or 300–400). The air from higher altitudes has a lower $^7\text{Be}/^{22}\text{Na}$ ratio due to lower production ratio and longer residence time. A longer residence time allows more ^7Be to decay than ^{22}Na , thus decreasing the ratio even more. In a simplified case, in winter the stagnant mixing conditions in the troposphere reduce the vertical transport of air masses. Thus the observed $^7\text{Be}/^{22}\text{Na}$ ratio at ground level is high due to production in low altitudes and short tropospheric residence time. Toward the summer the troposphere becomes more mixed due to the increasing amount of solar radiation causing convective flows in the atmosphere. In addition, the transport of stratospheric air masses through the tropopause increases. Thus more air from the upper troposphere and from the stratosphere mixes with ground-level air reducing the observed $^7\text{Be}/^{22}\text{Na}$ ratio. This agrees with the conclusions of Bourcier et al. (2011) who studied ^7Be activities simultaneously at different altitudes in France and concluded that differences in summer and winter ^7Be activities are caused by stronger vertical atmospheric mixing during summer.

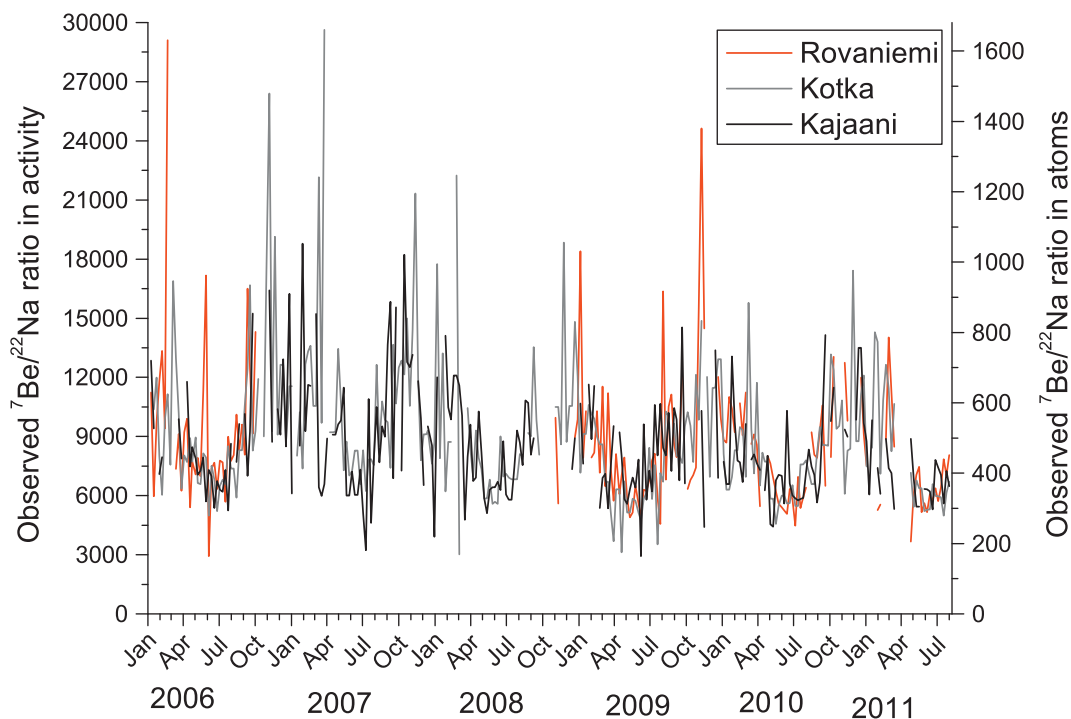


Fig. 12. The ^7Be and ^{22}Na activity ratio in weekly aerosol samples at Kotka, Kajaani and Rovaniemi from January 2006 to July 2011. The left y-axis shows the $^7\text{Be}/^{22}\text{Na}$ ratio in activity, while the right y-axis shows the $^7\text{Be}/^{22}\text{Na}$ ratio in atoms.

The ${}^7\text{Be}/{}^{22}\text{Na}$ ratio can work as a radiochronometer to estimate residence times of aerosols carrying cosmogenic isotopes. Table 3 lists theoretical production ratios of ${}^7\text{Be}/{}^{22}\text{Na}$ as a function of atmospheric depth. The difference between the observed ${}^7\text{Be}/{}^{22}\text{Na}$ ratios and calculated ones was significant as seen from Figs. 2 and 12. Assuming $200\text{--}600\text{ g/cm}^2$ as the atmospheric depth at the production altitude, the observed ${}^7\text{Be}/{}^{22}\text{Na}$ ratios at ground level were 3–8 times lower. This indicates long residence times of aerosols carrying ${}^7\text{Be}$ and ${}^{22}\text{Na}$ before reaching ground level. Roughly, the residence times must be of the order of a few times the half-life of ${}^7\text{Be}$. If the altitude of origin and residence time are known, residence time of the aerosols carrying cosmogenic isotopes could be estimated. However, this was not done in the framework of this study. In order to obtain more realistic residence time estimations production models need to be coupled with atmospheric models, e.g. GCM model, in a similar manner to Usoskin et al. (2009).

The use ${}^7\text{Be}/{}^{22}\text{Na}$ ratio as atmospheric tracer suffers from the low ${}^{22}\text{Na}$ activities. Thus more sensitive measurement systems are needed for an accurate determination of ${}^{22}\text{Na}$. The study of Zhang et al. (2010) presents the $\gamma\text{--}\gamma$ coincidence method where the ${}^{22}\text{Na}$ detection sensitivity from aerosol samples has been improved.

6. Conclusions

This study shows that in high latitudes the ambient air ${}^7\text{Be}$ activity is affected by climatic phenomena. The impact of different climatic phenomena on ${}^7\text{Be}$ activity was found to be sensitive to location. The changes in air mass transport patterns associated with NAO and AMO were determined to be the main contributor to the interannual variability of surface air ${}^7\text{Be}$ activities in Finland, whereas other studied climatic phenomena had less influence. The NAO and AMO have an influence due to their connection to precipitation and thus scavenging of aerosols carrying cosmogenic isotopes. The ${}^7\text{Be}$ and ${}^{22}\text{Na}$ activities were found to behave differently since ${}^{22}\text{Na}$ was less affected by climatic phenomena. The best example of this behavior is the lack of 4–8-year periodicity in the coherence between the ${}^{22}\text{Na}$ data and the NAO or AMO indices.

The ${}^7\text{Be}/{}^{22}\text{Na}$ ratio was suggested as a radiochronometer in atmospheric dynamics and a complementary method to ${}^{10}\text{Be}/{}^7\text{Be}$ ratio. The model calculations for the ${}^{22}\text{Na}$ and ${}^7\text{Be}/{}^{22}\text{Na}$ ratios in the low-middle atmosphere and lookup tables of ${}^{22}\text{Na}$ production in the atmosphere by cosmic rays are presented, as computed by the CRAC:22Na model. The ${}^7\text{Be}/{}^{22}\text{Na}$ ratios showed distinctive annual variation where generally low ratios were observed during summer and high ratios during winter. This is most likely connected to atmospheric mixing where air with a lower ${}^7\text{Be}/{}^{22}\text{Na}$ ratio originates from higher altitudes. Thus the observed ${}^7\text{Be}/{}^{22}\text{Na}$ ratio at ground level was dependent on the production altitude and residence time.

Acknowledgments

The CWT and WCA software package used in this study was provided by Dr. Aslak Grinsted. Dr. John Moore is acknowledged for providing additional help in the course of this study. The work and help of Mr. Pertti Niskala and Mrs. Riitta Kontro of the Radiation and Nuclear Safety Authority is acknowledged for updating and providing the data of the Ivalo, Rovaniemi, Kajaani and Kotka stations. GK acknowledges visiting grant from the Academy of Finland.

References

- Aldahan, A., Hedfors, J., Possnert, G., Kulan, A., Berggren, A., Söderström, C., 2008. Atmospheric impact on beryllium isotopes as solar activity proxy. *Geophysical Research Letters* 35, L21812.
- Aldahan, A., Possnert, G., Vintersved, I., 2001. Atmospheric interactions at northern high-latitudes from weekly Be-isotopes in surface air. *Applied Radiation and Isotopes* 54, 345–353.
- Baldwin, M., Dunkerton, T., 2001. Stratospheric harbingers of anomalous weather regimes. *Science* 294, 581–584.
- Bhandari, N., Lal, D., Rama, D., 1966. Stratospheric circulation studies based on natural and artificial radioactive tracer elements. *Tellus* 18, 391–406. doi:10.1111/j.21533490.1966.tb00250.x.
- Bourcier, L., Masson, O., Laj, P., Pichon, J.M., Paulat, P., Freney, E., Sellegri, K., 2011. Comparative trends and seasonal variation of ${}^7\text{Be}$, ${}^{210}\text{Pb}$ and ${}^{137}\text{Cs}$ at two altitude sites in the central part of France. *Journal of Environmental Radioactivity* 102 (3), 294–301.
- Cooke, D., Humble, J., Shea, M., Smart, D., Lund, N., Rasmussen, I., Byrnek, B., Goret, P., Petrou, N., 1991. On cosmic-ray cut-off terminology. *Nuovo Cimento C* 14, 213–234.
- El-Hussein, A., Ahmed, A., 1994. Activity size distribution of natural radionuclides. *Radiation Physics and Chemistry* 44, 99–101.
- Fassò, A., Ferrari, A., Ranft, J., Sala, P.R., 2001. FLUKA: Status and Prospective for Hadronic Applications, Invited talk in the Proceedings of the Monte Carlo 2000 Conference, Lisbon, October 23–26 2000, A. Kling, F. Barao, M. Nakagawa, L. Tavora, P. Vaz (Eds.), Springer-Verlag Berlin, pp. 955–960.
- Feely, H.W., Larsen, R.J., Sanderson, C.G., 1989. Factors that cause seasonal variations in beryllium-7 concentrations in surface air. *Journal of Environmental Radioactivity* 9, 223–249.
- Field, C., Schmidt, G., Koch, D., Salyk, C., 2006. Modeling production and climate-related impacts on ${}^{10}\text{Be}$ concentration in ice cores. *Journal of Geophysical Research* 111, D15107.
- Gerasopoulos, E., Zerefos, C., Papastefanou, C., Zanis, P., O'Brien, K., 2003. Low-frequency variability of beryllium-7 surface concentrations over the eastern Mediterranean. *Atmospheric Environment* 37, 1745–1756.
- Grabowska, S., Mietelski, J., Kozak, K., Gaca, P., 2003. Gamma emitters on microbecquerel activity level in air at Kraków (Poland). *Journal of Atmospheric Chemistry* 46, 103–116.
- Greatbatch, R., 2000. The North Atlantic oscillation. *Stochastic Environmental Research and Risk Assessment* 14, 213–242.
- Grinsted, A., Moore, J.C., Jevrejeva, S., 2004. Application of the cross wavelet transform and wavelet coherence to geophysical time series. *Nonlinear Processes in Geophysics* 11, 561–566.
- Heck, D., Knapp, J., Capdevielle, J., Schatz, G., Thouw, T., 1998. Corsika: a Monte Carlo code to simulate extensive air showers. In: FZKA 6019. Forschungszentrum, Karlsruhe.
- Hedfors, J., Aldahan, A., Kulan, A., Possnert, G., Karlsson, K.-G., Vintersved, I., 2006. Clouds and ${}^7\text{Be}$: perusing connections between cosmic rays and climate. *Journal of Geophysical Research* 111, D02208.
- Heikkilä, U., Beer, J., Feichter, J., 2009. Meridional transport and deposition of atmospheric ${}^{10}\text{Be}$. *Atmospheric Chemistry and Physics* 9, 515–527.
- Hubeny, J., King, J., Santos, A., 2006. Subdecadal to multidecadal cycles of late holocene North Atlantic climate variability preserved by estuarine fossil pigments. *Geology* 34, 569–572.
- Jasilionis, R., Wershofen, H., 2005. A study of the vertical diffusion of the cosmogenic radionuclides, ${}^7\text{Be}$ and ${}^{22}\text{Na}$ in the atmosphere. *Journal of Environmental Radioactivity* 79 (2), 157–169.
- Jevrejeva, S., Moore, J., 2001. Singular spectrum analysis of baltic sea ice conditions and large-scale atmospheric patterns since 1708. *Geophysical Research Letters* 28 (23), 4503–4506.
- Jevrejeva, S., Moore, J., Grinsted, A., 2003. Influence of the Arctic oscillation and El Niño-Southern Oscillation (ENSO) on ice conditions in the baltic sea: the wavelet approach. *Journal of Geophysical Research* 108, 4677.
- Jevrejeva, S., Moore, J., Grinsted, A., 2004. Oceanic and atmospheric transport of multiyear El Niño-Southern Oscillation (ENSO) signatures to the polar regions. *Geophysical Research Letters* 31, L24210.
- Jevrejeva, S., Moore, J., Grinsted, A., 2007. ENSO signal propagation detected by wavelet coherence and mean phase coherence methods. In: Tsonis, A., Elsner, J. (Eds.), *Nonlinear Dynamics in Geosciences*. Springer-Verlag, Berlin, pp. 167–175.
- Johnson, W., Viezee, W., 1981. Stratospheric ozone in the lower troposphere: i. Presentation and interpretation of aircraft measurements. *Atmospheric Environment* 15, 1309–1323.
- Jordan, C.E., Dibb, J.E., Finkel, R.C., 2003. ${}^{10}\text{Be}/{}^7\text{Be}$ tracer of atmospheric transport and stratosphere-troposphere exchange. *Journal of Geophysical Research* 108 (April), 4234.
- Kasatkina, E., Shumilov, O., Krapiec, M., 2007. On periodicities in long term climatic variations near 68°N 30°E . *Advanced Geosciences* 13, 25–29.
- Kikuchi, S., Sakurai, H., Gunji, S., Tokanai, F., 2009. Temporal variation of ${}^7\text{Be}$ concentrations in atmosphere for 8 y from 2000 at Yamagata, Japan: solar influence on the ${}^7\text{Be}$ time series. *Journal of Environmental Radioactivity* 100, 515–521.
- Knudsen, M., Seidenkrantz, M.-S., Jacobsen, B., Kuipers, A., 2011. Tracking the Atlantic multidecadal oscillation through the last 8,000 years. *Nature Communications* 2, 178.

- Koch, D., Mann, M., 1996. Spatial and temporal variability of ^7Be surface concentrations. *Tellus* 48B, 387–396.
- Kovaltsov, G.A., Usoskin, I.G., 2010. A new 3D numerical model of cosmogenic nuclide ^{10}Be production in the atmosphere. *Earth and Planetary Science Letters* 291, 182–188.
- Kulan, A., Aldahan, A., Possnert, G., Vintersved, I., 2006. Distribution of ^7Be in surface air of Europe. *Atmospheric Environment* 40, 3855–3868.
- Lal, D., Maholtra, P., Peters, B., 1958. On the production of radioisotopes in the atmosphere by cosmic radiation and their application to meteorology. *Journal of Atmospheric and Terrestrial Physics* 12, 306–328.
- Lal, D., Peters, B., 1962. Cosmic ray produced isotopes and their application to problems in geophysics. In: Wilson, J., Wouthuysen, S. (Eds.), *Progress in Elementary Particle and Cosmic Ray Physics*, vol. 6. , North Holland, Amsterdam, pp. 77–243.
- Leppänen, A.-P., Grinsted, A., 2008. Observations of cosmogenic ^7Be and ^{22}Na in aerosol samples in Northern Finland. In: Paschoa, A., Steinäusler, F. (Eds.), *The Natural Radiation Environment, 8th International Symposium (NRE VIII)*, AIP Conference Proceedings, vol. 1034; 2008, pp. 112–115.
- Leppänen, A.-P., Pacini, A., Usoskin, A., Echer, E., Evangelista, H., Klemola, S., Kovaltsov, G., Mursula, K., Possnert, G., 2010. Cosmogenic ^7Be in air: a complex mixture of production and transport. *Journal of Atmospheric and Solar-Terrestrial Physics* 72, 1036–1043.
- Luyanas, V., 2004. Cosmogenic Radionuclides in the Atmosphere. MOKSLAS, Vilnius (in Russian).
- Masarik, J., Beer, J., 1999. Simulation of particle fluxes and cosmogenic nuclide production in the earth's atmosphere. *Journal of Geophysical Research* 104, 12099–12111.
- Mattsson, R., Helminen, V., Sucksdorff, C., 1965. Some investigations of airborne radioactivity with a view to meteorological applications. *Finnish Meteorological Office Contributions*, vol. 58. , Finnish Meteorological Office, Helsinki, pp. 53.
- Medici, F., 2001. Particulate sampling in the IMS radionuclide network of the Comprehensive-Nuclear Test Ban Treaty. *Kerntechnik* 66, 121–125.
- O'Brien, K., 1979. Secular variations in the production of cosmogenic isotopes in the earth's atmosphere. *Journal of Geophysical Research* 84, 423–431.
- Paatero, J., Hatakka, J., 2000. Airborne ^7Be and ^{210}Pb measured in Northern Finland. *Health Physics* 79 (6), 692–696.
- Paatero, J., Hatakka, J., Mattsson, R., Aaltonen, V., Viisanen, Y., 2000. Long-term variations of ^{210}Pb concentrations in ground-level air in Finland: effects of the North Atlantic oscillation. In: Midgley, P., Reuther, M., Williams, M. (Eds.), *Transport and Chemical Transformation in the Troposphere: Proceedings of the EUROTRAC-2 Symposium 2000*. , Springer-Verlag, Berlin, Germany, pp. 322–324.
- Papastefanou, C., Ioannidou, A., 1995. Aerodynamic size association of Be-7 in ambient aerosols. *Journal of Environmental Radioactivity* 26, 273–282.
- Partal, T., 2010. Wavelet analysis and multi-scale characteristics of the runoff and precipitation series of the Aegean region (Turkey). *International Journal of Climatology*. doi:10.1002/joc.2245.
- Poore, R., DeLong, K., Richey, J., Quinn, T., 2009. Evidence of multidecadal climate variability and the Atlantic multidecadal oscillation from a Gulf of Mexico sea-surface temperature-proxy record. *Geo-Marine Letters* 29, 477–484.
- Raisbeck, G., Yiou, F., Fruneau, M., Loiseaux, J., Lieuvin, M., Ravel, J., 1981. Cosmogenic Be-10/Be-7 as a probe of atmospheric transport processes. *Geophysical Research Letters* 8, 1015–1018.
- Raspovop, O., Dergachev, V., Kolstöm, T., 2004. Periodicity of climate conditions and solar variability derived from dendrochronological and other paleoclimatic data in high latitude. *Palaeogeography, Palaeoclimatology, Palaeoecology* 209, 127–139.
- Reyss, J.-L., Yokoyama, Y., Guichard, F., 1981. Production cross sections of ^{26}Al , ^{22}Na , ^7Be from argon and of ^{10}Be , ^7Be from nitrogen: implications for production rates of ^{26}Al and ^{10}Be in the atmosphere. *Earth and Planetary Science Letters* 53, 203–210.
- Rodwell, M., Rowell, D., Folland, C., 1999. Oceanic forcing of the wintertime North Atlantic oscillation and European climate. *Nature* 398, 320–323.
- Rulík, P., Malá, H., Becková, V., Hölgue, Z., Schlesingerová, E., Svetlík, I., Skral, J., 2009. Low level air radioactivity measurements in Prague, Czech Republic. *Applied Radiation and Isotopes* 67, 969–973.
- Silberberg, R., Tsao, C.H., 1973. Partial cross-sections in high-energy nuclear reactions, and astrophysical applications. I. Targets with $z \leq 28$. *Astrophysical Journal Supplement* 25, 315–333.
- Simon, J., Meresova, J., Sykora, I., Jeskovsky, M., Holy, K., 2009. Modeling of temporal variations of vertical concentration profile of ^7Be in the atmosphere. *Atmospheric Environment* 43 (12), 2000–2004.
- Talpos, S., Rimbu, N., Borsan, D., 2005. Solar forcing on the ^7Be -air concentration variability at ground level. *Journal of Atmospheric and Solar-Terrestrial Physics* 67, 1626–1631.
- Tatischeff, V., Kozlovsky, B., Kiener, J., Murphy, R.J., 2006. Delayed x- and gamma-ray line emission from solar flare radioactivity. *Astrophysical Journal Supplement Series* 165 (August), 606–617.
- Tokuyama, H., Igarashi, S., 1998. Seasonal variation in the environmental background level of cosmic-ray-produced ^{22}Na at Fukui city, Japan. *Journal of Environmental Radioactivity* 38 (2), 147–161.
- Torrence, C., Compo, G., 1998. A practical guide to wavelet analysis. *Bulletin of the American Meteorological Society* 79, 61–78.
- Usoskin, I., Kovaltsov, G., 2008. Production of cosmogenic ^7Be isotope in the atmosphere: full 3D modelling. *Journal of Geophysical Research* 113, D12107.
- Usoskin, I.G., Alanko-Huotari, K., Kovaltsov, G.A., Mursula, K., 2005. Heliospheric modulation of cosmic rays: monthly reconstruction for 1951–2004. *Journal of Geophysical Research* 110, A12108.
- Usoskin, I.G., Bazilevskaya, G., Kovaltsov, G.A., 2011. Solar modulation parameter for cosmic rays since 1936 reconstructed from ground-based neutron monitors and ionization chambers. *Journal of Geophysical Research* 116 (A02104), 9. doi:10.1029/2010JA016105.
- Usoskin, I.G., Field, C.V., Schmidt, G.A., Leppänen, A.-P., Aldahan, A., Kovaltsov, G.A., Possnert, G., Ungar, R.K., 2009. Short-term production and synoptic influences on atmospheric ^7Be concentrations. *Journal of Geophysical Research* 114 (D13), D06108.
- Vecchi, R., Valli, G., 1997. ^7Be in surface air: a natural atmospheric tracer. *Journal of Aerosol Science* 28 (5), 895–900.
- Velasco, V., Mendoza, B., 2008. Assessing the relationship between solar activity and some large scale climatic phenomena. *Advances in Space Research* 47, 866–878.
- Webber, W., Higbie, P., McCracken, K., 2007. Production of the cosmogenic isotopes ^3H , ^7Be , ^{10}Be , and ^{36}Cl in the earth's atmosphere by solar and galactic cosmic rays. *Journal of Geophysical Research* 112, A10106.
- Weyhenmeyer, G., Blenckner, T., Petterson, K., 1999. Changes of the plankton spring outburst related to the North Atlantic oscillation. *Limnology and Oceanography* 44, 1788–1792.
- Zhang, W., Yi, J., Mekarski, P., Hoffman, I., Ungar, K., Leppänen, A.-P., 2010. A system for low-level the cosmogenic ^{22}Na radionuclide measurement by gamma-gamma coincidence method using BGO detector. *Journal of Radio-analytical and Nuclear Chemistry* 287, 551–555.